

1
MOD DEC 10 1947
Restriction/Classification Cancelled

Westinghouse
24C/1
RM No. SETJ06

Source of Acquisition
CASI Acquired

~~CLASSIFIED~~
~~RESTRICTED~~
~~CONFIDENTIAL~~
~~SECURITY INFORMATION~~
~~NACA~~
~~Dr. James H. Doolittle~~
~~NACA~~
~~CCS~~
~~NACA changed 1454~~

RESEARCH MEMORANDUM

for the

Bureau of Aeronautics, Navy Department

SIMULATED ALTITUDE PERFORMANCE OF COMBUSTORS

FOR THE 24C JET ENGINE

II - 24C-4 COMBUSTOR

By Everett Bernardo, Thomas T. Schroeter
and Robert C. Miller

Flight Propulsion Research Laboratory
Cleveland, Ohio

RESTRICTED
CONFIDENTIAL
Restriction/
Classification
Cancelled

~~CLASSIFIED~~
~~RESTRICTED~~
~~CONFIDENTIAL~~

This document contains classified information affecting the National Defense of the United States within the meaning of the Espionage Act, USC 50:31 and 32. Its transmission or the revelation of its contents in any manner to an unauthorized person is prohibited by law. Information so classified may be imparted only to personnel in the military and naval Services of the United States, appropriate civilian officers and employees of the Federal Government who have a legitimate interest therein, and to United States citizens of known loyalty and discretion who of necessity must be informed thereof.

TECHNICAL
EDITING
WAIVED

~~CONFIDENTIAL~~
~~RESTRICTED~~
~~CONFIDENTIAL~~
~~SECURITY INFORMATION~~
~~NACA~~
~~Dr. James H. Doolittle~~
~~NACA~~
~~CCS~~
~~NACA changed 1454~~
~~2463~~
~~status: Insensitive~~

NATIONAL ADVISORY COMMITTEE FOR AERONAUTICS

WASHINGTON

NOV 12 1947

FILE COPY

To be returned to
the files of the National
Advisory Committee

for Aeronautics
Washington, D. C.

Restriction/Classification Cancelled

CONFIDENTIAL
CLASSIFICATION CANCELLED

NATIONAL ADVISORY COMMITTEE FOR AERONAUTICS

RESEARCH MEMORANDUM

for the

Bureau of Aeronautics, Navy Department

SIMULATED ALTITUDE PERFORMANCE OF COMBUSTORS

FOR THE 24C JET ENGINE

II - 24C-4 COMBUSTOR

By Everett Bernardo, Thomas T. Schroeter
and Robert C. Miller

SUMMARY

The performance of a 24C-4 combustor was investigated with three different combustor baskets and five modifications of these baskets at conditions simulating static (zero-ram) operation of the 24C jet engine over ranges of altitude and engine speed to determine and improve the altitude operational limits of the 24C combustor. Information was also obtained regarding combustion characteristics, the fuel-flow characteristics of the fuel manifolds, and the combustor total-pressure drop.

NACA modifications, which consisted of blocking rows of holes on the baskets, increased the minimum point on the altitude-operational-limit curve, which occurs at low engine speeds, for a narrow-upstream-end basket by 8000 feet (from 23,000 to 31,000 ft) and for a wide-upstream-end basket by 21,000 feet (from 13,000 to 34,000 ft). These improvements were approximately maintained over the entire range of engine speeds investigated.

INTRODUCTION

At the request of the Bureau of Aeronautics, Navy Department, the NACA Cleveland laboratory has cooperated with the Westinghouse Electric Corporation in the investigation and the improvement of the performance of combustors for turbojet engines. The altitude performance of 24C-2, 19B, and 9.5A combustors is presented in references 1, 2, and 3, respectively, and investigations of NACA modifications for improving the altitude performance of the 9.5B combustor are reported in reference 4.

CONFIDENTIAL
CLASSIFICATION CANCELLED

The altitude performance of a 24C-4 combustor using three different combustor baskets and a total of five modifications of these baskets is presented. The performance was investigated in a manner similar to that of reference 1 (24C-2 combustor). Ranges of simulated altitudes and engine speeds were investigated with each of the three baskets to determine the altitude operational limits as indicated by the ability of the combustor to provide exhaust gases of the temperatures required by the turbine for engine operation and the effect of each of the five modifications on the altitude operational limits was ascertained. In addition, information was obtained regarding the general operation of the combustor and the character of the flames, the combustion efficiency, the combustor-outlet gas temperature and velocity distributions, the fuel-flow characteristics of the fuel manifolds, the combustor total-pressure drop, and the condition of the baskets after running.

COMBUSTOR

A longitudinal section of the 24C-4 combustor and the immediate auxiliary ducting used is shown in figure 1. The combustor is similar to the 24C-2; the chief differences are that the 24C-4 combustor is approximately $1\frac{1}{2}$ inches larger in diameter ($25\frac{1}{2}$ in. I. D.), $1\frac{9}{32}$ inches longer ($24\frac{3}{32}$ in.), and has a correspondingly larger basket than the 24C-2 combustor.

Diagrams of the longitudinal sections and hole arrangements of the three baskets, which were supplied by the manufacturer, are presented in figure 2. Each basket consists of two tapered concentric annular chambers having mean diameters of approximately $14\frac{3}{8}$ and $21\frac{7}{8}$ inches, respectively. The annular chambers are approximately $13\frac{19}{32}$ inches long and $3\frac{1}{4}$ inches wide at the downstream end. For admitting air into the basket, the shells of each of the chambers are perforated with holes that progressively increase in diameter downstream. Each shell of the chambers is equipped with stiffener rings. The width of the chambers at the upstream end and other pertinent features of the three baskets are listed in the following table:

Config-uration	Figure	Location and type of stiffeners	Basket width at upstream section (in.)	Number of rows of holes lengthwise	Diameter of holes (in.)
1	2(a)	Flame side, angular	$1\frac{1}{2}$	20	$\frac{5}{32} - \frac{5}{8}$
2	2(a)	Antiflame side, band	$1\frac{1}{2}$	20	$\frac{5}{32} - \frac{5}{8}$
a ₃	2(b)	Antiflame side, band	$2\frac{1}{4}$	19	$\frac{7}{32} - \frac{5}{8}$

^aAlso has 372 holes (ram-pressure air holes) of 1/8-inch diameter at upstream end.

Configuration 1, which was not altered, is the same as configuration 2 (narrow-upstream-end baskets) except for the type of stiffener used. (See fig. 2(a).) The modifications of configuration 2 and configuration 3 (wide-upstream-end basket) are shown diagrammatically in figure 3 and listed in the following table:

Configuration	Figure	Type of modification
2A	3(a)	Rows of holes in basket blocked
3A	3(b)	Ram-pressure air holes blocked
3B	3(b)	Configuration 3A plus streamlined approach
3C	3(c)	Configuration 3A plus rows of holes in basket blocked
3D	3(c)	Configuration 3C plus streamlined approach

The ram-pressure air holes were blocked with short screws and annular sheet-metal fairings were used to streamline the approach to the basket. (See figs. 3(b) and 3(c).) The rows of holes in the baskets were blocked by welding strips of Inconel to the baskets approximating the arrangement that resulted in the greatest improvement of the altitude operational limits in an unpublished investigation conducted by the NACA on a 1/8 segment of a 19B combustor.

The percentage of the total open area as a function of the distance downstream for each of the basket configurations investigated is shown in figure 4. For configurations 1, 2, 3, 3A, and 3B, the percentage of open area increases rather uniformly with the distance downstream. For configurations 2A, 3C, and 3D, however, only about 14 to 18 percent of the total open area occurs in the first two-thirds of the basket.

Each of the two annular chambers of the basket was provided with a fuel manifold and the same manifolds were used throughout the investigation. A total of 60 hollow-cone-spray fuel-injection nozzles (45° spray angle, 5 gal/hr at a pressure differential of 100 lb/sq in.) was used, 36 on the outer and 24 on the inner manifold. The fuel was supplied to the manifolds through separate inlets located at the bottom of the combustor. Fuel flow was measured with a calibrated rotameter and fuel pressure was measured at the junction of the inlets to the manifolds with a calibrated Bourdon gage.

Bench tests of the manifolds conducted at frequent intervals during the investigation indicated a maximum individual deviation from the average fuel flow of approximately 10 and 17 percent at fuel-manifold differential pressures of 100 and 5 pounds per square inch, respectively. The manifolds were mounted vertically (as in the combustor) during the bench tests and, as in reference 1, the flow from the bottom nozzles was noted to be slightly higher than that from the top nozzles, which indicates that gravity affected the flow distribution.

APPARATUS

A diagram of the general setup (essentially that described in reference 1) is shown in figure 5. Combustion air (which was metered with a variable-area orifice), altitude exhaust, and fuel (AN-F-28, Amendment-2) were provided by the laboratory systems. Combustion-air flow and pressure were controlled through regulating valves and the temperature of the combustion air was regulated by means of electric air heaters and a fuel-fired preheater. Windows were provided for observation of the flames. A plenum chamber, a punched plate, and a screen installed in the setup provided uniform velocity and temperature distributions at the inlet to the combustor.

Temperature and Pressure Instrumentation

Temperature- and pressure-measuring instruments were located at five sections (A-A to E-E) shown in figure 1. The sections are designated as follows: combustor inlet, A-A; fuel-nozzle plane, B-B; and combustor outlet, C-C (corresponding to turbine-inlet section of engine); instrumentation was installed at sections D-D and E-E to check for afterburning. The orientation of the instruments in the various sections is illustrated in figure 6. The

construction details of the instruments and the methods of measuring pressures and temperatures were as described in reference 1. The radial spacing and the details of the instruments at sections A-A and B-B, which differ slightly from the arrangement used in reference 1, are shown in figure 7. The use of the instrumentation at sections B-B and D-D was discontinued after runs with configuration 1.

METHODS

The altitude operation of a 24C-4 combustor using each of the three production baskets (configurations 1, 2, and 3) and the five modified configurations (2A and 3A to 3D) was investigated with combustor-inlet air conditions of weight flow, temperature, and pressure simulating static (zero-ram) operation of the turbojet engine at various altitudes from sea level to at least 50,000 feet and for a range of simulated engine speeds from 4000 to 12,000 rpm.

Isothermal runs were conducted using each of the configurations to provide additional data on the variation of total-pressure drop in the combustor with air flow.

The combustor-inlet air conditions of weight flow, temperature, and pressure and the values of the estimated combustor-outlet temperatures required for operation of the 24C jet engine were furnished by the manufacturer and are the same as those presented in reference 1. Inlet-air conditions were kept within 1 percent of their estimated required values.

Ignition of a fuel-air mixture in the combustor was obtained within the following range of conditions:

Air flow, lb/sec	2 - 3
Inlet pressure, in. Hg gage	-3 - 4
Fuel flow, lb/hr	200 - 250

After ignition was obtained, the combustion-air flow and inlet-air temperature were set while the fuel flow was adjusted to maintain combustion. The inlet pressure, initially higher than desired, was then reduced to its proper value. Finally, in the operational-limit runs the fuel flow was gradually increased while all other conditions were maintained constant in an effort to obtain an average combustor-outlet temperature equal to or greater than the value required for operation of the turbojet engine at the particular condition. Operable engine conditions were those at which required

combustor-outlet temperatures were attained; inoperable engine conditions were those at which the required combustor-outlet temperatures were unobtainable. During the efficiency runs the fuel flow was set at various selected values.

The methods of calculation are the same as those of reference 1. Average temperatures and pressures were taken as the average of all the respective readings at each section, and average inlet and outlet velocities were calculated from measured air flows and areas, average static pressures, and average temperatures at sections A-A and C-C, respectively. The local outlet-gas velocities used to obtain the velocity distributions were calculated from the individual probe total-pressure indications, the wall-static pressures adjacent to each total-pressure rake, and the local temperatures interpolated from the indications of the adjacent thermocouple rakes. Fuel-manifold pressure differential was taken as the difference between the measured fuel-manifold pressure corrected for elevation to the center of the manifold and the average static pressure at section C-C. The combustion efficiency is defined as the ratio of the average gas-temperature rise through the combustor to the temperature rise theoretically obtainable with the same fuel-air ratio. Values of the theoretical temperature rise were obtained from reference 5 for a fuel having a lower heating value of 18,700 Btu per pound and a hydrogen-carbon ratio of 0.175.

The effective dynamic pressure q was calculated from the combustion-air flow, the average inlet-air temperature and static pressure, and the maximum cross-sectional area of the combustor (420 sq in.), which in the setup is equal to the cross-sectional area at section A-A; hence, q is equal to the dynamic pressure at the inlet for the setup used.

RESULTS AND DISCUSSION

Altitude Operational Results

The altitude operational limits (at zero ram) for each of the configurations investigated are presented in figure 8 in plots of simulated altitude against simulated engine speed. In each plot the altitude operational limits are defined by a curve that separates the inoperable region where required combustor-outlet temperatures could not be obtained from the operable region where the required combustor-outlet temperatures were attainable. At several conditions with configuration 2, the required combustor-outlet

temperatures were exceeded but blow-outs prevented operation at the values of the required temperatures. These points are therefore listed as inoperable. (See fig. 8(b).)

The altitude-operational-limit curves of figure 8 are compared in figure 9 and the altitude operational limits attained with the 24C-2 combustor (reference 1) are included. The altitude operational limits for each of the 24C-4 configurations are higher than those for the 24C-2 except for configuration 1 at an engine speed of 12,000 rpm. This increase in operational limits is attributed in part to the lower velocities resulting from the increased cross-sectional areas of the 24C-4 combustor and basket.

The following table lists the minimum critical altitudes and their corresponding engine speeds for the various configurations studied. The minimum critical altitude is defined as the minimum point on the altitude-operational-limit curve. The engine speed at which an altitude operational limit of 50,000 feet was obtained is also listed.

Config- uration	Minimum critical altitude (ft)	Engine speed at minimum critical altitude (rpm)	Engine speed for altitude operational limit of 50,000 feet (rpm)
1	23,000	4500	10,100
2	23,000	4500	10,800
2A	31,000	5000	9,000
3	13,000	4000	10,800
3A	18,000	4000	10,600
3B	18,000	4000	10,600
3C	34,000	4000	9,000
3D	34,000	4000	9,000
^a 24C-2	9,000	6000	12,000

^aData from reference 1.

The minimum critical altitude for each configuration of the 24C-4 combustor studied occurred at engine speeds of between 4000 and 5000 rpm. Configuration 2A, in which rows of holes on the basket were blocked (fig. 3(a)), provided an increase of 8000 feet in minimum critical altitude over configuration 2. The minimum critical altitude was 10,000 feet lower for configuration 3 than

for configurations 1 and 2 in spite of the increased width of the annular chambers and resultant lower velocities in configuration 3. Configuration 3A, in which the ram-pressure air holes were blocked (fig. 3(b)), provided an increase of 5000 feet in the minimum critical altitude over configuration 3; configuration 3B, in which streamlined approach mounted on the fuel manifolds was also added (fig. 3(b)), provided no further improvement. Configuration 3C, in which rows of holes on the basket were blocked (fig. 3(c)), provided an increase in minimum critical altitude of 21,000 feet over that of configuration 3. The addition of the streamlined approach to configuration 3C (configuration 3D) had no discernible effect on the operational limits. The minimum critical altitudes for the configurations of the 24C-4 combustor investigated are from 4000 to 25,000 feet higher than that for the 24C-2 combustor.

The improvements in the operational limits at the engine speeds corresponding to the minimum critical altitude were approximately maintained over the entire engine speed range investigated. Because 50,000 feet was about the maximum altitude investigated, however, the improvements at high engine speeds are indicated by a reduction in the speed at which an altitude limit of 50,000 feet was attained.

Character of Flames

Over most of the range of conditions investigated, three general types of combustion, similar to those described in reference 1, were observed: steady, flickering, and cycling. Flickering combustion usually marked the transition from steady to cycling combustion although the distinction between the types of flame was not always pronounced. The inception of cycling combustion was generally accompanied by a drop in combustor-outlet temperature. Increasing the fuel-air ratio during cycling increased the combustor-outlet temperature but at a slower rate than that obtained during steady combustion. Cycling combustion was usually encountered before blow-outs.

In general, the combustion was steady at conditions at which the required combustor-outlet temperature was either attained or exceeded, and the combustion was flickering or cycling at conditions at which the required outlet temperature was unattainable. In several runs, particularly with configuration 2, however, higher outlet temperatures were attained during cycling than during steady combustion.

The color of the flames was observed to vary with increasing altitude from yellow or yellow-white to blue, with orange or red

flames sometimes observed at intermediate altitudes. Yellow flames were often observed at high altitudes during cycling combustion.

The effect of fuel-air ratio on combustion near the operational limits was determined with configuration 1. The combustion was observed to change from steady to cycling with increasing fuel-air ratio until blow-out occurred, and from cycling to steady with decreasing fuel-air ratio.

The combustion with configuration 2A was steadier than that obtained with configuration 2. In configuration 3, the flames failed to seat on the walls of the basket, and dark spaces often appeared in the combustion zone. These irregularities were reduced somewhat in configuration 3A and practically eliminated in configuration 3C. The use of the streamlined approach in configurations 3B and 3D had no appreciable effect on combustion.

In general, the combustion in all configurations investigated was quieter, and cycling, when encountered, was milder than that described for the 24C-2 combustor in reference 1.

Temperature Rise across Combustor and Combustion Efficiency

The variation of the temperature rise across the combustor with fuel-air ratio for simulated operation at normal and military rated engine speeds (11,000 and 12,000 rpm, respectively) and at various altitudes is presented in figure 10 for configuration 3C. The combustor temperature rise required for engine operation is indicated on each curve. At a given altitude and engine speed, the temperature rise increased with an increase in fuel-air ratio for the range of fuel-air ratios investigated, the rate of increase decreasing slightly with fuel-air ratio. In several runs (not shown in fig. 10) close to the operational limits, however, the combustor temperature rise was observed to attain a maximum value and thereafter decrease with a further increase in fuel-air ratio.

For the same data as those of figure 10, the variation of combustion efficiency with fuel-air ratio is shown in figure 11. The fuel-air ratio required for engine operation is indicated on each curve. For the range of fuel-air ratios investigated, the combustion efficiency changed inappreciably. For comparable fuel-air ratios, the combustion efficiency decreased with increasing altitude and decreasing engine speed. This variation is representative of all the configurations investigated.

For conditions below the altitude operational limits at which the required combustor-outlet temperatures were attained, the combustion efficiencies were of the order of 95 percent at the lowest altitudes investigated but decreased to values as low as 40 percent at the higher altitudes. The combustion efficiencies of configurations 2A and 3C were slightly higher than those of configurations 2 and 3 for corresponding altitude and engine-speed conditions. The other modifications made to configuration 3 resulted in no appreciable improvement in combustion efficiency over the unmodified configuration.

At conditions above the operational limits, combustion efficiencies were usually below 60 percent although some higher efficiencies were recorded, particularly with configuration 2.

Combustor-Outlet Temperatures and Velocities

Temperature distribution. - Several typical combustor-outlet temperature distributions for steady and cycling combustion conditions are shown in figures 12 and 13 in both polar- and rectangular-coordinate plots. Figure 12 illustrates the temperature distributions obtained with configuration 1 for a relatively low engine speed (6000 rpm) during steady combustion below the operational limit and during cycling combustion above the operational limit. The spread between the maximum and minimum temperatures was 45 percent of the average temperature rise during steady combustion, but during cycling combustion the spread increased to 134 percent of the average temperature rise.

Temperature patterns for high combustor-inlet air temperature conditions (approximately 280° F) for an engine speed of 12,000 rpm and an altitude of 50,000 feet are shown in figure 13 as obtained with configurations 2 and 2A. These patterns are similar to those for altitudes down to 35,000 feet and engine speeds of 12,000 rpm. The difference between the maximum and minimum temperatures for the unmodified basket (configuration 2) was 105 percent of the average temperature rise but in configuration 2A the difference was 150 percent of the average temperature rise. The increase in deviation over the unmodified basket is attributed, in part, to a change in air distribution resulting from the blocked holes and to a change in air distribution caused by warping of the basket during the welding of the hole-blocking strips.

The temperatures in the upper portion of the combustor for both configurations 2 and 2A were relatively low at high inlet-air

temperatures. This condition is attributed to the effect of fuel vaporization in the upper portion of the manifold, which is discussed later. The effect was more pronounced with configuration 2 than with configuration 2A.

Blocking the ram-pressure air holes (configuration 3A) and the use of the streamlined approach (configurations 3B and 3D) had no appreciable effect on the temperature distributions.

For corresponding conditions, the temperature distributions for configurations 1, 2, and 3 were similar to and appreciably better than those reported in reference 1 for the 24C-2 combustor, especially at high inlet-air temperatures. The improvement is attributed to the increased fuel pressure resulting from the use of fuel nozzles of smaller capacity (5 gal/hr compared with 7.5 gal/hr for the 24C-2 combustor) and the subsequent improvement in fuel distribution.

Velocity distribution. - Typical velocity distributions at the combustor outlet for steady and cycling combustion are presented in figure 14 (configuration 1) at the same conditions as those for figure 12. The velocities peaked at about 1 inch from the outer wall; the greatest spread in the velocities was roughly 120 feet per second in each case, from 355 to 475 feet per second during steady combustion and from 275 to 395 feet per second during cycling combustion.

Indications of afterburning. - No evidence of appreciable afterburning was obtained with any of the original basket configurations. A comparison of the average gas temperatures at sections D-D and E-E with the average combustor-outlet gas temperatures at section C-C is shown in figure 15 for configuration 1. The temperatures at each of the sections agreed within 25° F in most runs; however, indications of slight amounts of afterburning were evident for some runs.

The appearance of the flames during several runs with configurations 2A, 3C, and 3D indicated that, at very high altitudes with conditions adverse to combustion, appreciable afterburning occurred.

Fuel-Manifold Flow Characteristics

The flow characteristics of the fuel manifold as a function of the inlet-air temperature are shown in figure 16 for all the runs. The fuel flow W_f divided by the square root of the fuel-manifold

pressure differential ΔP_f is shown plotted against the fuel-manifold pressure for inlet-air temperatures below 150° F and of approximately 210° and 280° F. The exponent on ΔP_f is an average value obtained in the bench calibration of the manifolds.

There is appreciable scatter in the data but the effect of inlet-air temperature on the flow characteristics is evident. At inlet-air temperatures below 150° F, the fuel-manifold pressure has no appreciable effect on the value of $W_f/\Delta P_f^{0.5}$. At inlet-air temperatures of 210° and 280° F, however, the value of $W_f/\Delta P_f^{0.5}$ (and hence fuel flow for a given ΔP_f) decreases with decreasing fuel-manifold pressure; the decrease is greater at the higher temperature. This reduction in fuel flow was caused by fuel vaporization or deaeration in the upper portion of the manifold, which would, of course, be affected by both temperature and pressure. The adverse effect of the liberation of vapor or air from the upper nozzles on temperature distribution was illustrated in figure 13.

Correlation of Total-Pressure-Drop Data

A correlation of typical combustor inlet-to-outlet total-pressure-drop ΔP (sections A-A to C-C) with the ratio of inlet-to-outlet density ρ_A/ρ_C is presented in figure 17 for configuration 1, and a straight line is obtained that represents the data with a scatter of about ± 5 percent. Similar curves were obtained for the other configurations and all the curves are presented in figure 18. The values of $\Delta P/q$ for isothermal runs ($\rho_A/\rho_C = 1.0$) and for combustion runs ($\rho_A/\rho_C = 3.0$) are as follows:

Con- fig- ura- tion	Combustor total-pressure drop $\Delta P/q$ (in. Hg absolute)	
	$\rho_A/\rho_C = 1.0$	$\rho_A/\rho_C = 3.0$
1	5.0	8.9
2	5.0	8.7
2A	7.8	11.9
3	9.1	13.3
3A	9.9	13.7
3B	8.3	13.8
3C	13.8	20.6
3D	12.8	18.1

During combustion (at values of $\rho_A/\rho_C = 3.0$), the pressure drop of the wide-upstream-end basket (configuration 3) was approximately 50 percent greater than that of the narrow-upstream-end basket (configuration 2), and blocking holes on the baskets (configurations 2A, 3C, and 3D) increased the pressure drop by roughly 40 percent in each case.

The values of $\Delta P/q$ are lower for configurations 1 and 2 than those for the 24C-2 combustor, which had a lower maximum cross-sectional area (reference 2), but those for each version of configuration 3 are higher, being roughly 3.5 higher than those for configurations 1 and 2. The increases in pressure drop resulting from the blocking of basket holes in configurations 2A, 3A, and 3C are approximately $3q$, $0.7q$, and $3.8q$ to $7q$, respectively. The streamlined approach to the basket used in configurations 3B and 3D had no appreciable effect on the pressure drop. The increase in pressure drop obtained with configuration 3 is attributed to the greatly restricted air passages between the basket and the combustor walls resulting from the wide upstream end of the basket, and that obtained with configurations 2A, 3A, and 3C is attributed to the reduced basket-hole areas.

Condition of Baskets

A slight circumferential wrinkle developed in each shell of the baskets and the rust-colored deposit and the canary-yellow residue described in reference 1 were present on each basket. Configurations 2 and 3, with external stiffeners, were in better condition than configuration 1, in which the internal stiffener rings were burned. After modifications, however, configurations 2 and 3 warped severely under the hole-blocking strips.

SUMMARY OF RESULTS

The results of an investigation conducted with a 24C-4 combustor using three different baskets supplied by the manufacturer and five modifications of these baskets over large ranges of simulated altitudes and engine speeds indicated that:

1. Operation at zero ram of a 24C turbojet engine with the three unmodified baskets would be limited to altitudes ranging from 13,000 feet to 23,000 feet at engine speeds of 4000 and 4500 rpm, respectively. The operational limit would increase to an altitude of 50,000 feet at engine speeds ranging from 10,100 to 10,800 rpm.

2. NACA modifications, which consisted of blocking rows of holes on the baskets, increased the minimum point on the altitude-operational-limit curve, which occurs at low engine speeds, for a narrow-upstream-end basket by 8000 feet (from 23,000 to 31,000 ft) and for a wide-upstream-end basket by 21,000 feet (from 13,000 to 34,000 ft). The improvements were approximately maintained over the entire range of engine speeds investigated.

3. At conditions below the operational limits, the combustion efficiencies ranged from 95 percent at the lowest altitudes investigated to 40 percent at the higher altitudes; the NACA modifications slightly increased these efficiencies.

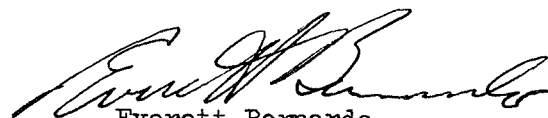
4. The maximum variations in the local combustor-outlet gas temperatures of the baskets ranged roughly from 45 percent to 150 percent of the average combustor temperature rise and were considerably smaller than those for the 24C-2 basket for similar operating conditions.

5. At conditions of high inlet-air temperature and low fuel pressure, fuel vapor or air was liberated in the upper fuel nozzles and adversely affected the combustor-outlet temperature distribution.


C-00000
0-00-00


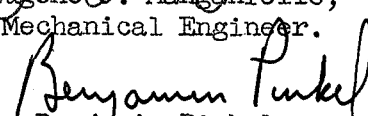
6. During combustion, the combustor inlet-to-outlet total-pressure drop of the wide-upstream-end basket was approximately 50 percent greater than that of the narrow-upstream-end basket, and blocking holes on the baskets increased the pressure drop by roughly 40 percent in each case.

Flight Propulsion Research Laboratory,
National Advisory Committee for Aeronautics,
Cleveland, Ohio.


Everett Bernardo,
Mechanical Engineer.

Thomas T. Schroeter,
Mechanical Engineer.


Robert C. Miller,
Mechanical Engineer.

Approved: 
Eugene J. Manganiello,
Mechanical Engineer.

Benjamin Pinkel,
Physicist.

rl

REFERENCES

1. Manganiello, Eugene J., Bernardo, Everett, and Schroeter, Thomas T.: Simulated Altitude Performance of Combustors for the Westinghouse 24C Jet Engine. I - 24C-2 Combustor. NACA RM No. E6J09, Bur. Aero., 1946.

2. Childs, J. Howard, McCafferty, Richard J., and Surine, Oakley W.: Effect of Combustor-Inlet Conditions on Performance of an Annular Turbojet Combustor. NACA TN No. 1357, 1947.
3. Manganiello, Eugene J., and Bogart, Donald: Simulated Altitude Performance of Combustors for the Westinghouse 9.5 Jet Engine. I - 9.5A Combustor. NACA MR No. E6F28, Bur. Aero., 1946.
4. Bogart, Donald: Simulated Altitude Performance of Combustors for the 9.5 Jet Engine. II - 9.5B Combustor. NACA RM No. E7B21, Bur. Aero., 1947.
5. Turner, L. Richard, and Lord, Albert M.: Thermodynamic Charts of the Computation of Combustion and Mixture Temperatures at Constant Pressure. NACA TN No. 1086, 1946.

INDEX OF FIGURES

Figure 1. - Longitudinal section of 24C-4 combustor showing auxiliary ducting and instrumentation planes.

Figure 2. - Diagrammatic sketch of basket-hole arrangements and longitudinal sections of 24C-4 combustor baskets.

(a) Configurations 1 and 2; narrow-upstream-end basket.

(b) Configuration 3; wide-upstream-end basket.

Figure 3. - Diagrammatic sketch of basket-hole arrangements and longitudinal sections of modifications to 24C-4 combustor baskets.

(a) Configuration 2A.

(b) Configurations 3A and 3B.

(c) Configurations 3C and 3D.

Figure 4. - Percentage of total open area of baskets for 24C-4 combustor.

(a) Configurations 1 and 2.

(b) Configuration 2A.

(c) Configuration 3.

(d) Configurations 3A and 3B.

(e) Configurations 3C and 3D.

Figure 5. - Diagrammatic sketch of setup for 24C combustor.

Figure 6. - Orientation of instrumentation in 24C-4 combustor looking upstream.

Figure 7. - Construction details of instrumentation at sections A-A and B-B of 24C-4 combustor.

Figure 8. - Altitude operational limits of 24C jet engine for zero ram as determined with 24C-4 combustor.

(a) Configuration 1, narrow-upstream-end basket equipped with angular stiffeners on flame side of each shell.

(b) Configuration 2, narrow-upstream-end basket equipped with bank stiffeners on antiframe side of each shell.

(c) Configuration 2A, rows of holes on basket blocked.

(d) Configuration 3, wide-upstream-end basket.

(e) Configuration 3A, ram-pressure air holes blocked, and configuration 3B, ram-pressure air holes blocked plus streamlined approach.

(f) Configuration 3C, ram-pressure air holes and rows of holes on basket blocked, and configuration 3D, streamlined approach plus configuration 3C.

Figure 9. - Comparison of altitude operational limits of 24C jet engine as obtained with 24C-4 combustor using various basket configurations and with 24C-2 combustor.

Figure 10. - Variation of average combustor temperature rise with fuel-air ratio for 24C-4 combustor, configuration 3C.

- (a) Engine speed, 11,000 rpm.
- (b) Engine speed, 12,000 rpm.

Figure 11. - Variation of combustion efficiency with fuel-air ratio for 24C-4 combustor, configuration 3C.

- (a) Engine speed, 11,000 rpm.
- (b) Engine speed, 12,000 rpm.

Figure 12. - Temperature distribution at combustor outlet (section C-C, looking upstream) during steady and cycling combustion for engine speed of 6000 rpm. 24C-4 combustor, configuration 1.

- (a) Radial and circumferential temperature distribution during steady combustion; altitude, 22,500 feet.
- (b) Radial temperature distribution during steady combustion; altitude, 22,500 feet.
- (c) Radial and circumferential temperature distribution during cycling combustion; altitude, 25,000 feet.
- (d) Radial temperature distribution during cycling combustion; altitude, 25,000 feet.

Figure 13. - Temperature distribution at combustor outlet (section C-C, looking upstream) for high inlet-air temperatures (approximately 280° F) at engine speed of 12,000 rpm and altitude of 50,000 feet. 24C-4 combustor, configurations 2 and 2A.

- (a) Configuration 2, radial and circumferential temperature distribution.
- (b) Configuration 2, radial temperature distribution.
- (c) Configuration 2A, radial and circumferential temperature distribution.
- (d) Configuration 2A, radial temperature distribution.

Figure 14. - Velocity distribution at combustor outlet (section C-C). 24C-4 combustor, configuration 1, at an engine speed of 6000 rpm.

Figure 15. - Relation of average temperature measured at sections D-D and E-E to average combustor-outlet temperature at section C-C. 24C-4 combustor, configuration 1.

- (a) Relation of average temperature measured at section D-D to average combustor-outlet temperature.
- (b) Relation of average temperature measured at section E-E to average combustor-outlet temperature.

Figure 16. - Fuel-manifold flow characteristics as function of inlet-air temperature. 24C-4 combustor.

Figure 17. - Correlation of combustor total-pressure drop. 24C-4 combustor, configuration 1.

Figure 18. - Comparison of combustor total-pressure drop for 24C-4 combustor baskets and modifications.

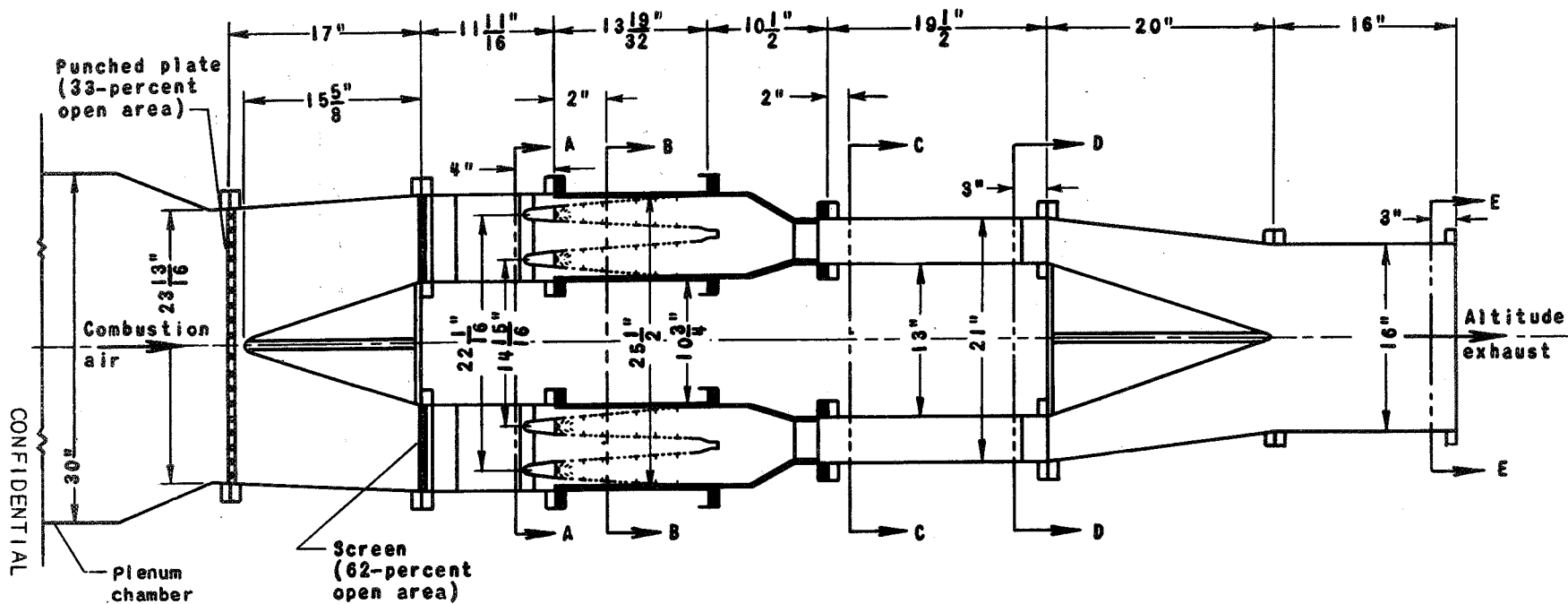


Figure 1. - Longitudinal section of 24C-4 combustor showing auxiliary ducting and instrumentation planes.

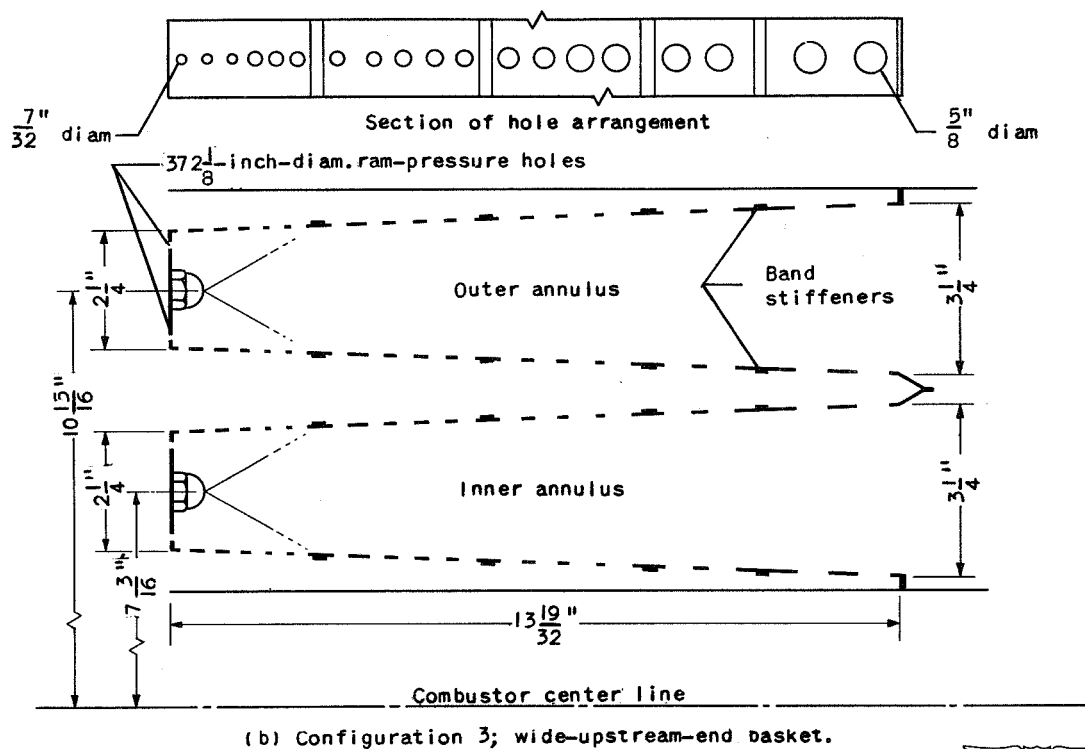
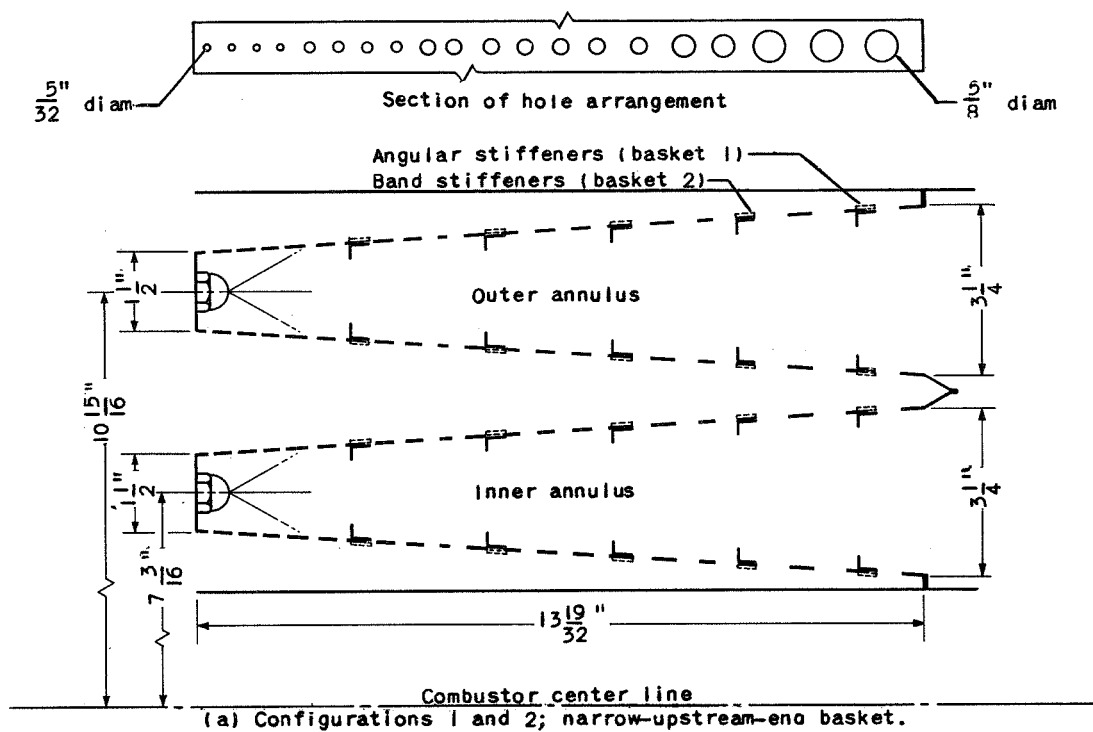


Figure 2. - Diagrammatic sketch of basket-hole arrangements and longitudinal sections of 24C-4 combustor baskets.

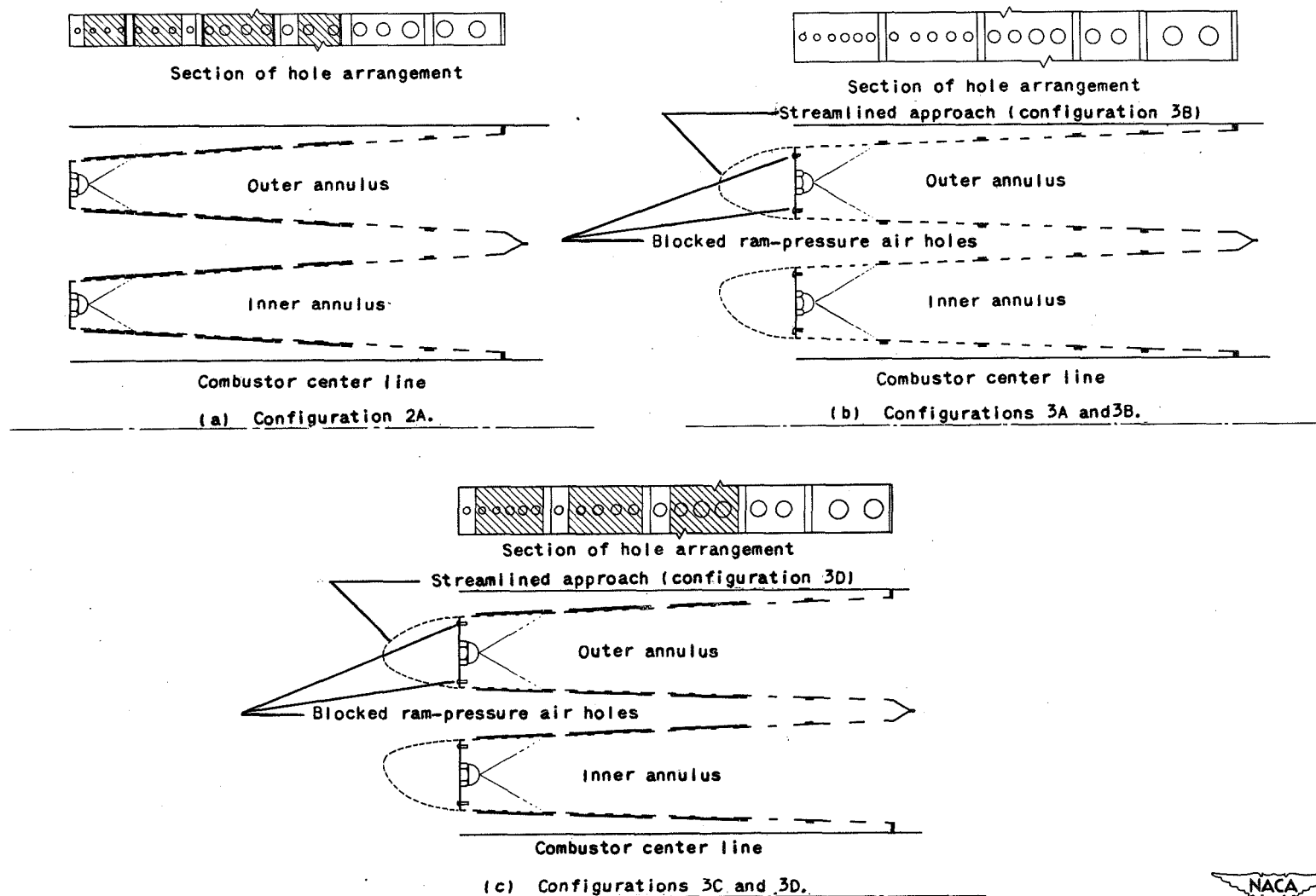


Figure 3. - Diagrammatic sketch of basket-hole arrangements and longitudinal sections of modifications to 24C-4 combustor baskets.

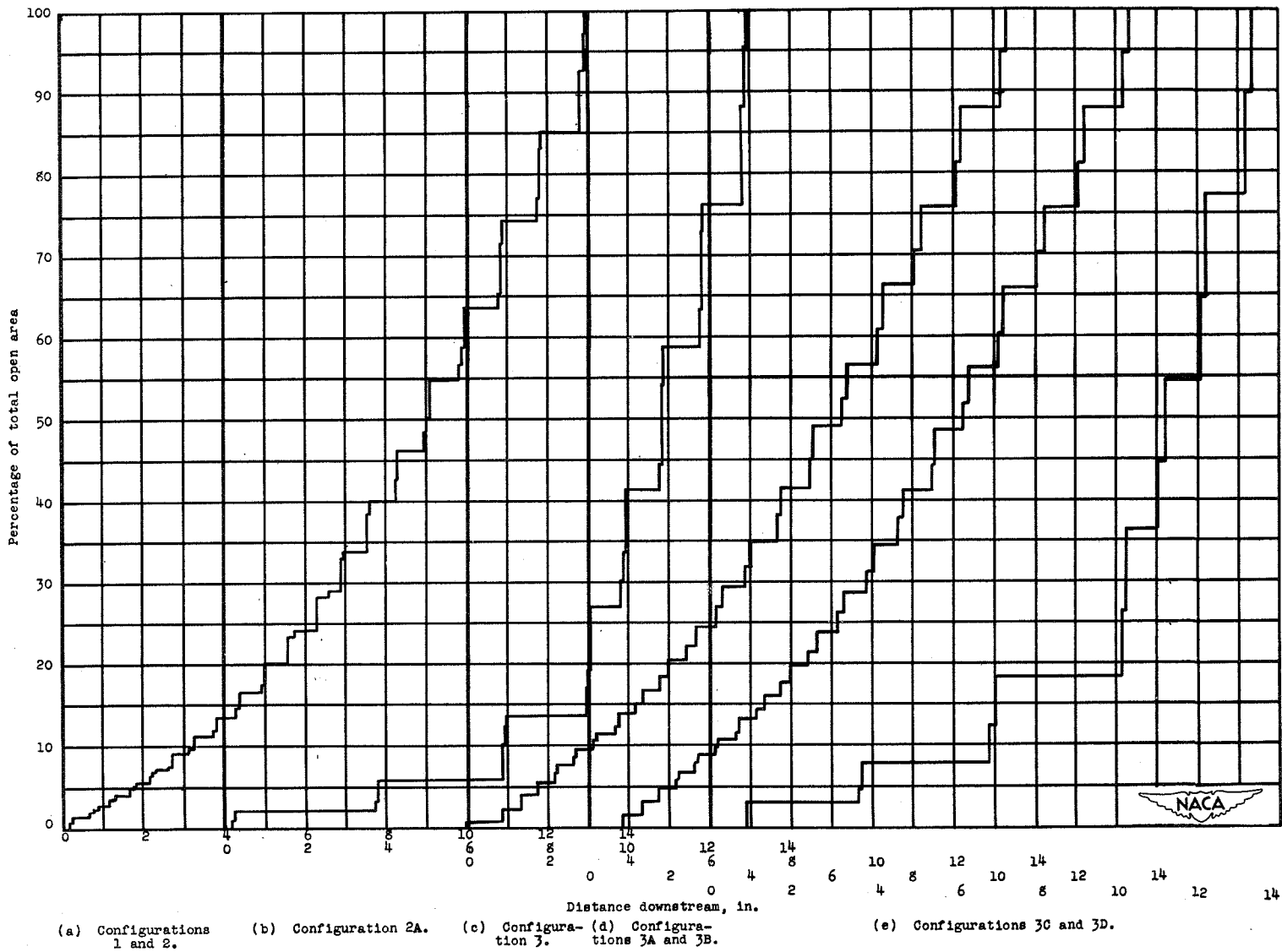


Figure 4. - Percentage of total open area of baskets for 24C-4 combustor.

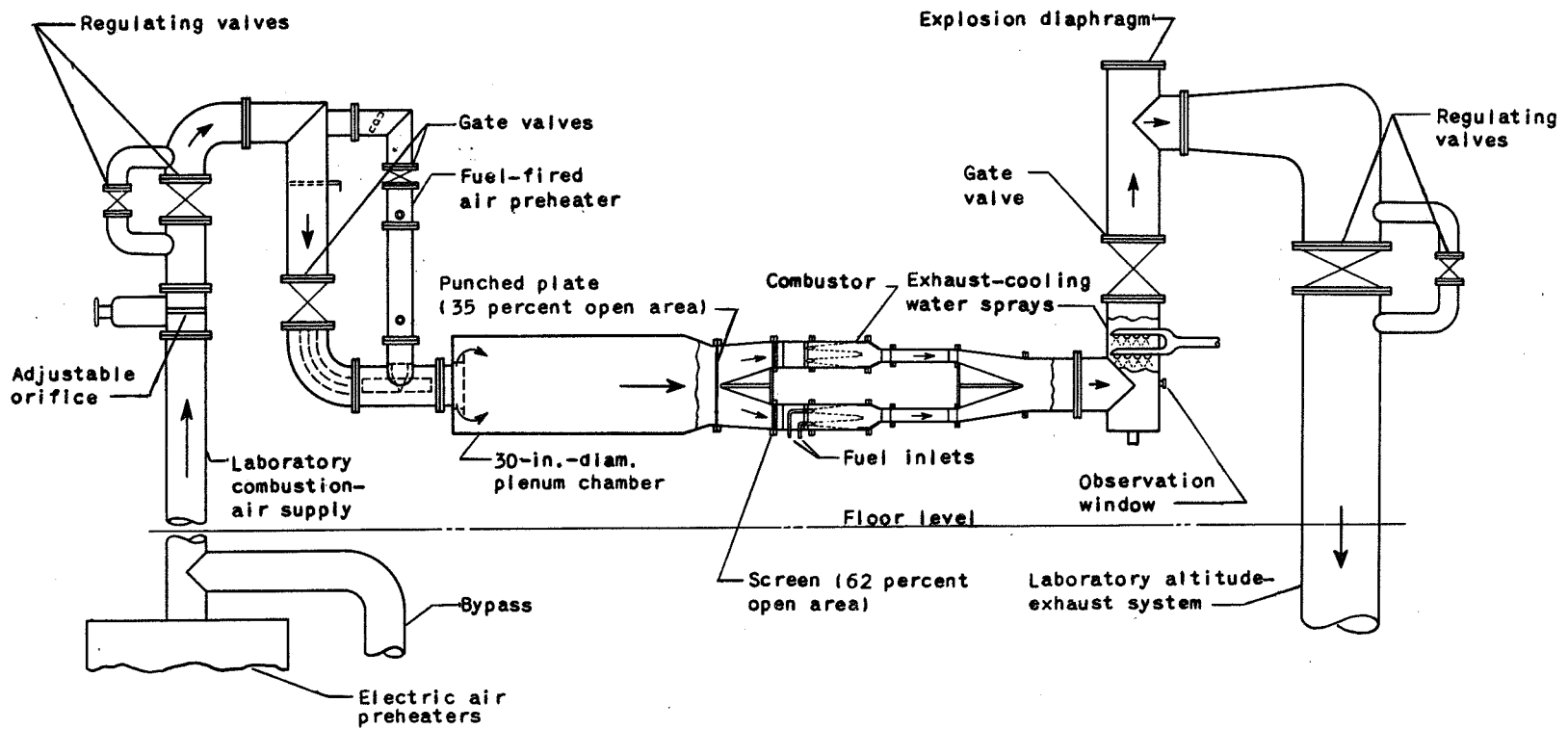


Figure 5. - Diagrammatic sketch of setup for 24C combustor.

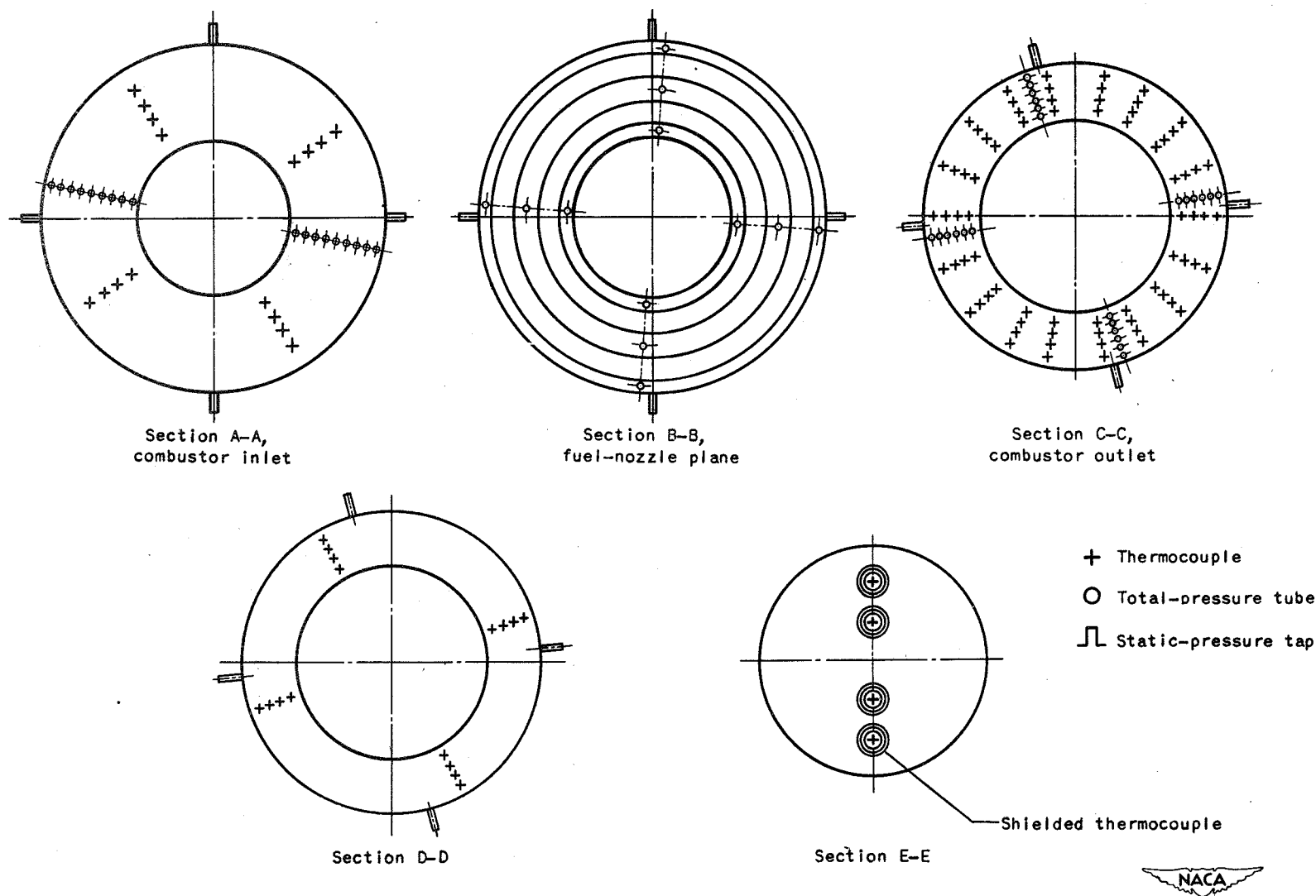


Figure 6. - Orientation of instrumentation in 24C-4 combustor looking upstream.

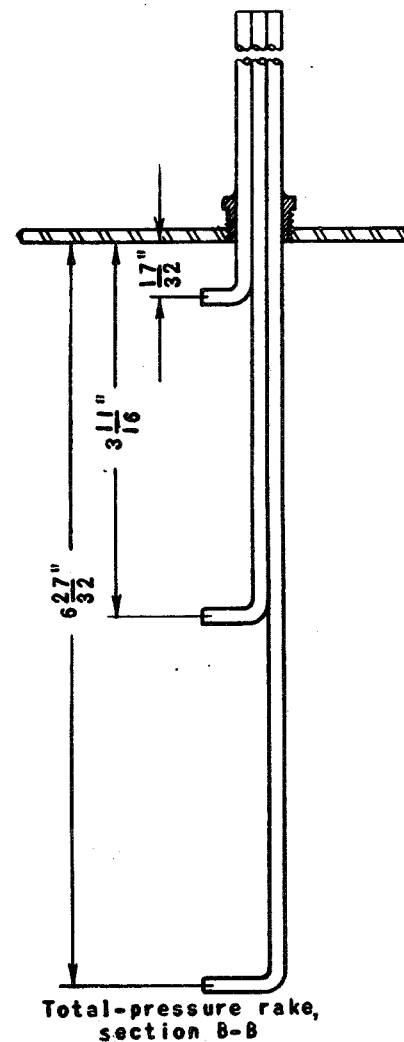
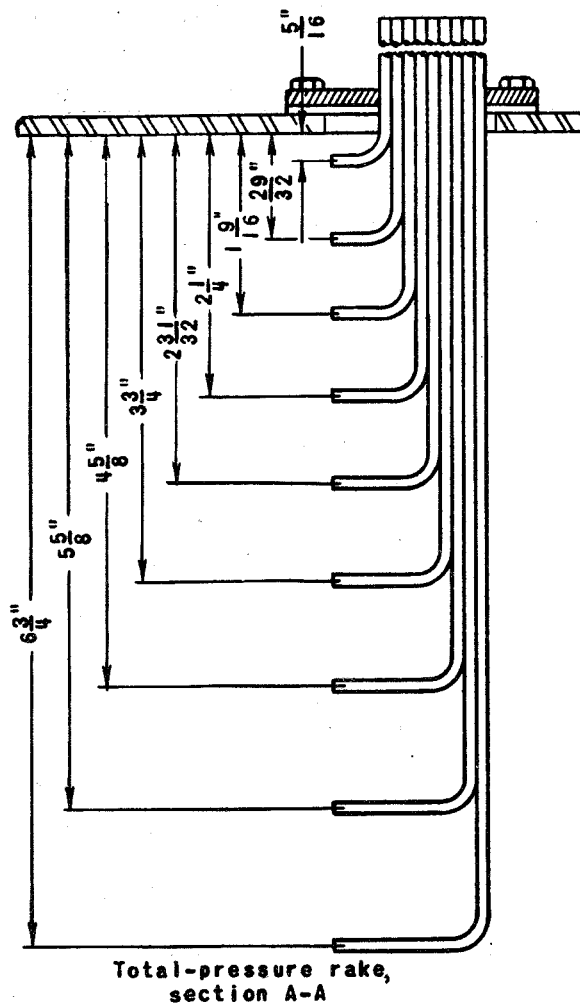
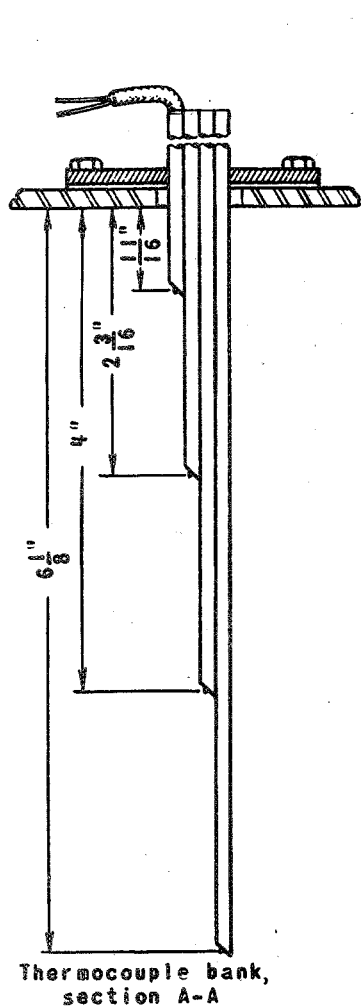
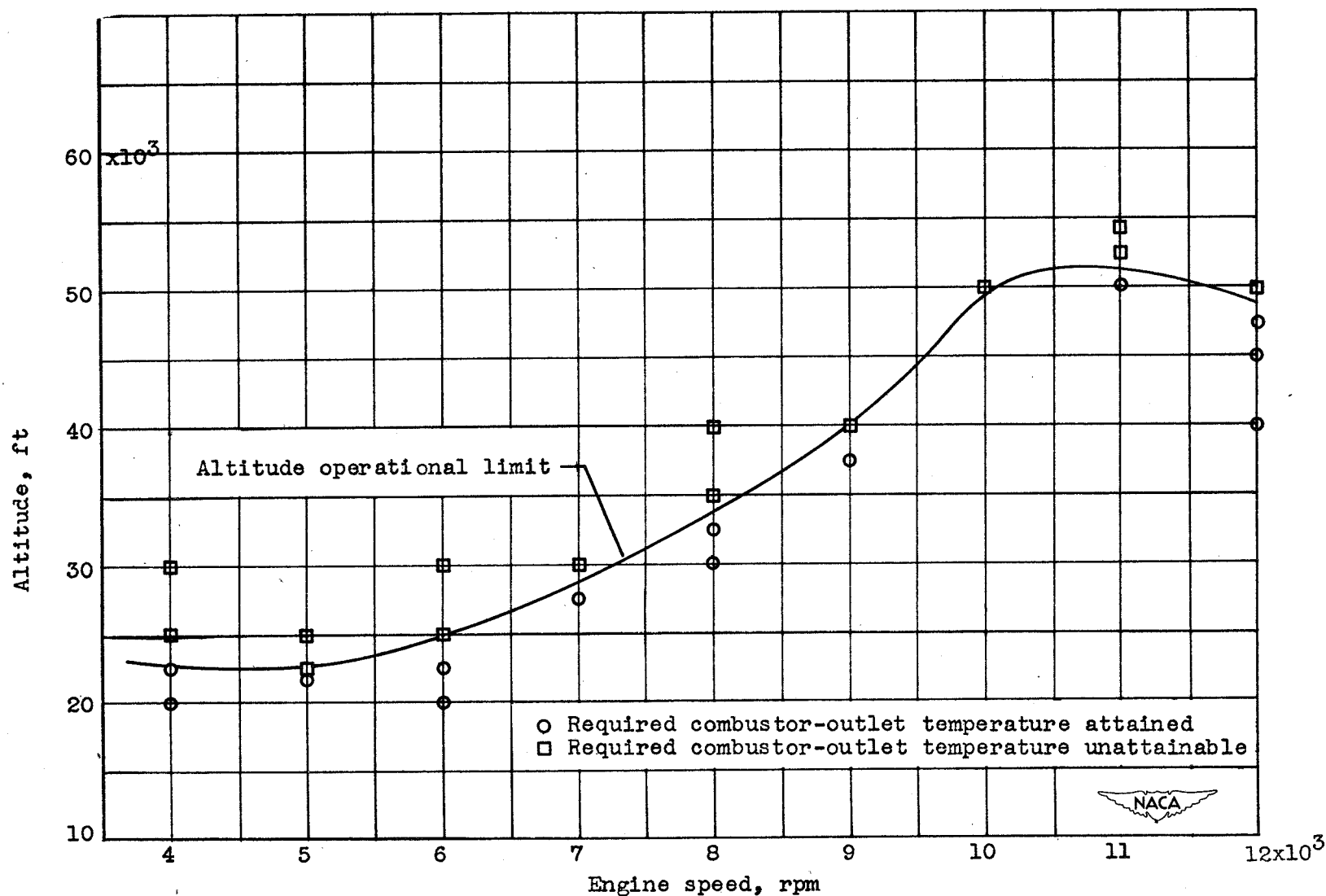
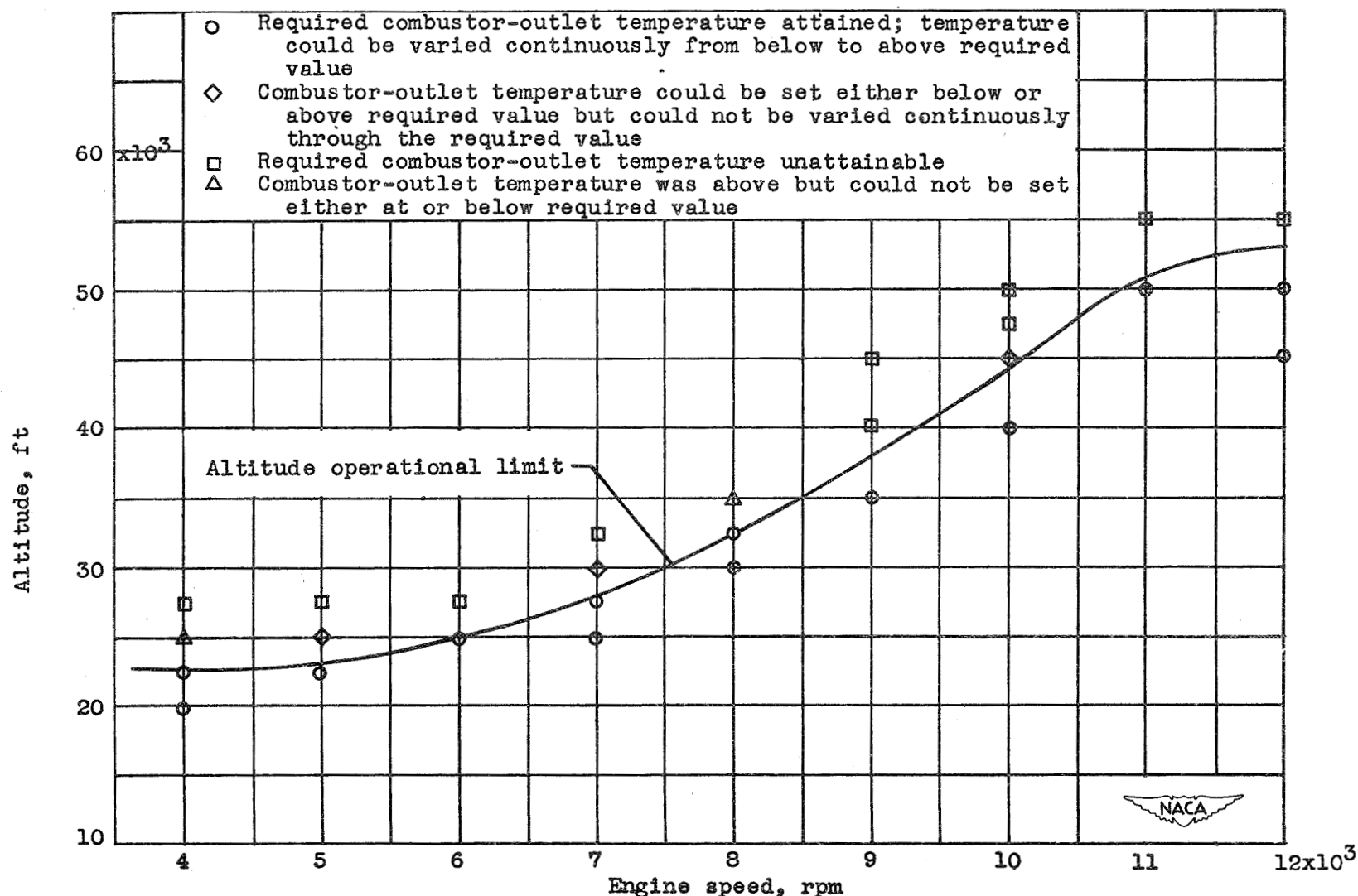


Figure 7. - Construction details of instrumentation at sections A-A and B-B of 24C-4 combustor.



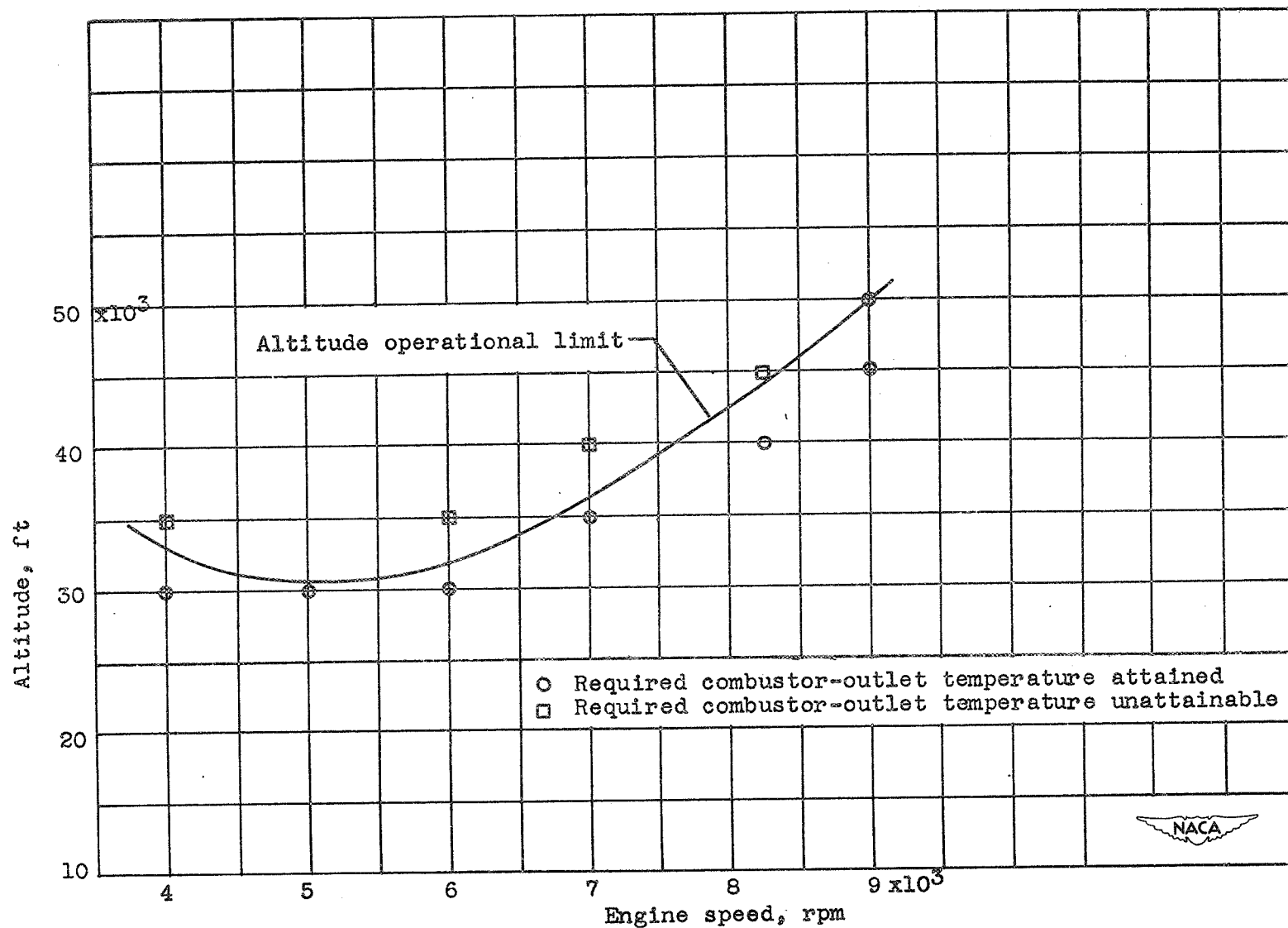
(a) Configuration 1, narrow-upstream-end basket equipped with angular stiffeners on flame side of each shell.

Figure 8. - Altitude operational limits of 24C jet engine for zero ram as determined with 24C-4



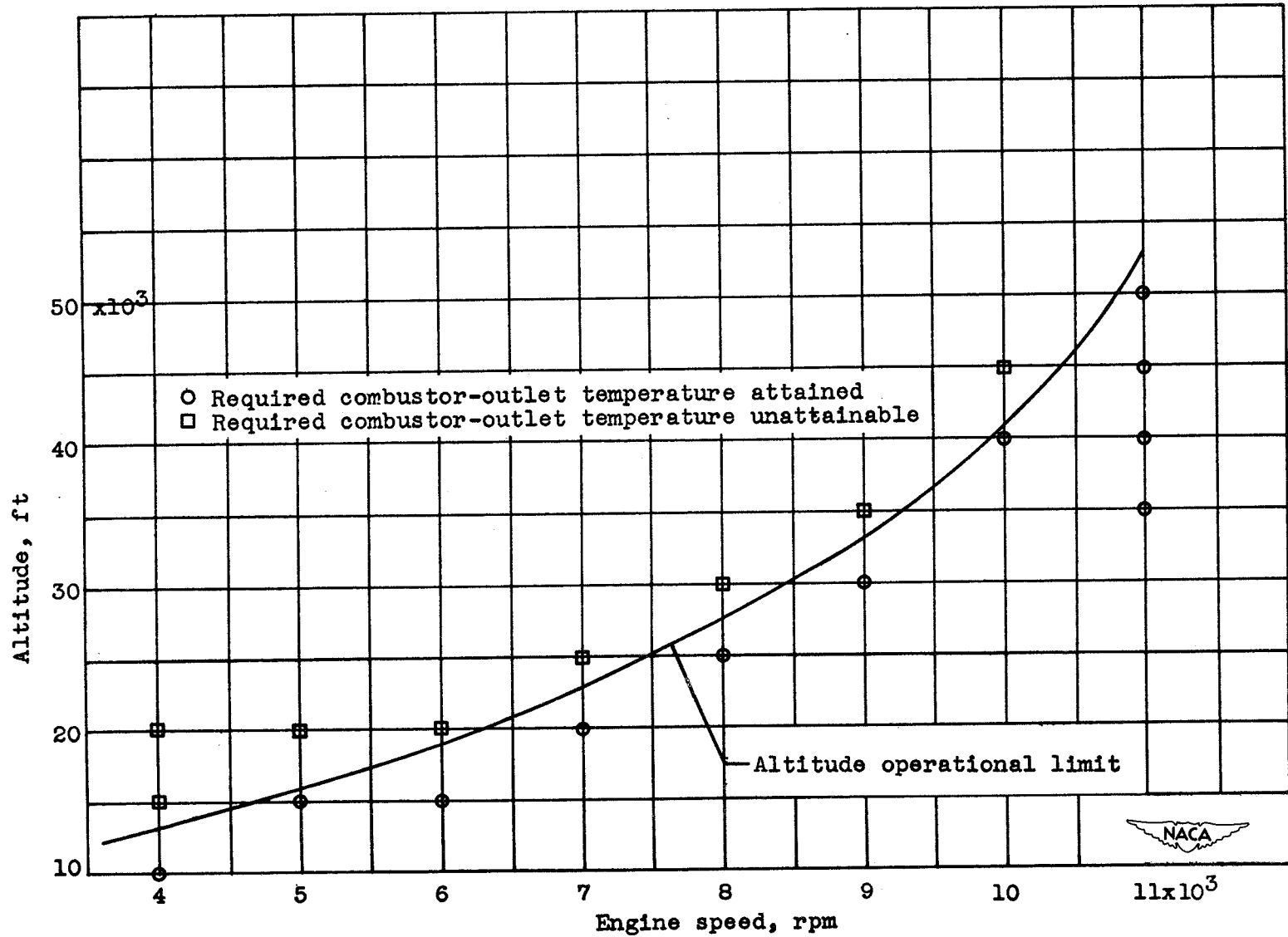
(b) Configuration 2, narrow-upstream-end basket equipped with band stiffeners on anti-flame side of each shell.

Figure 8. - Continued. Altitude operational limits of 24C jet engine for zero ram as determined with 24C-4 combustor.



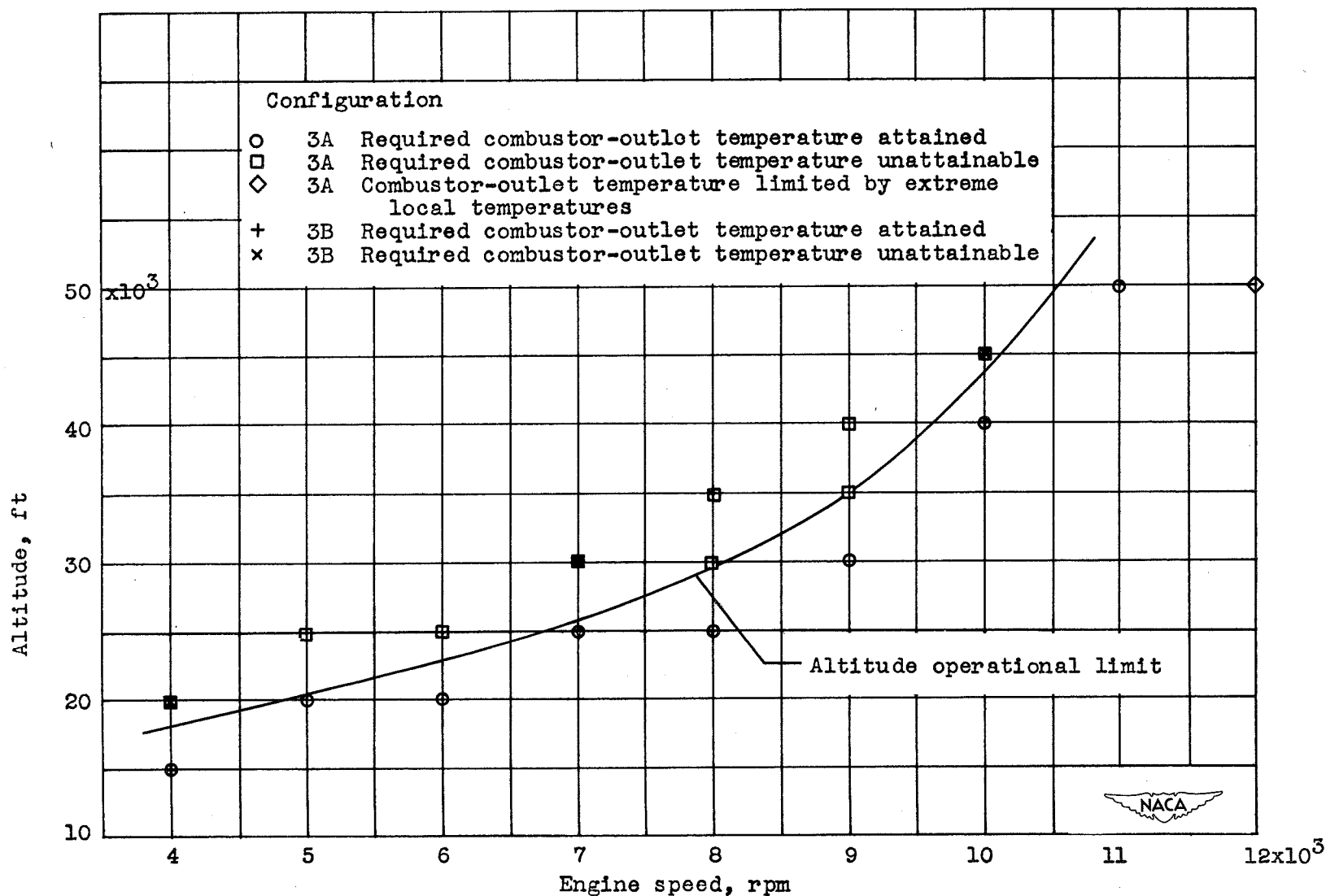
(c) Configuration 2A, rows of holes on basket blocked.

Figure 8. - Continued. Altitude operational limits of 24C jet engine for zero ram as determined with 24C-4 combustor.



(d) Configuration 3, wide-upstream-end basket.

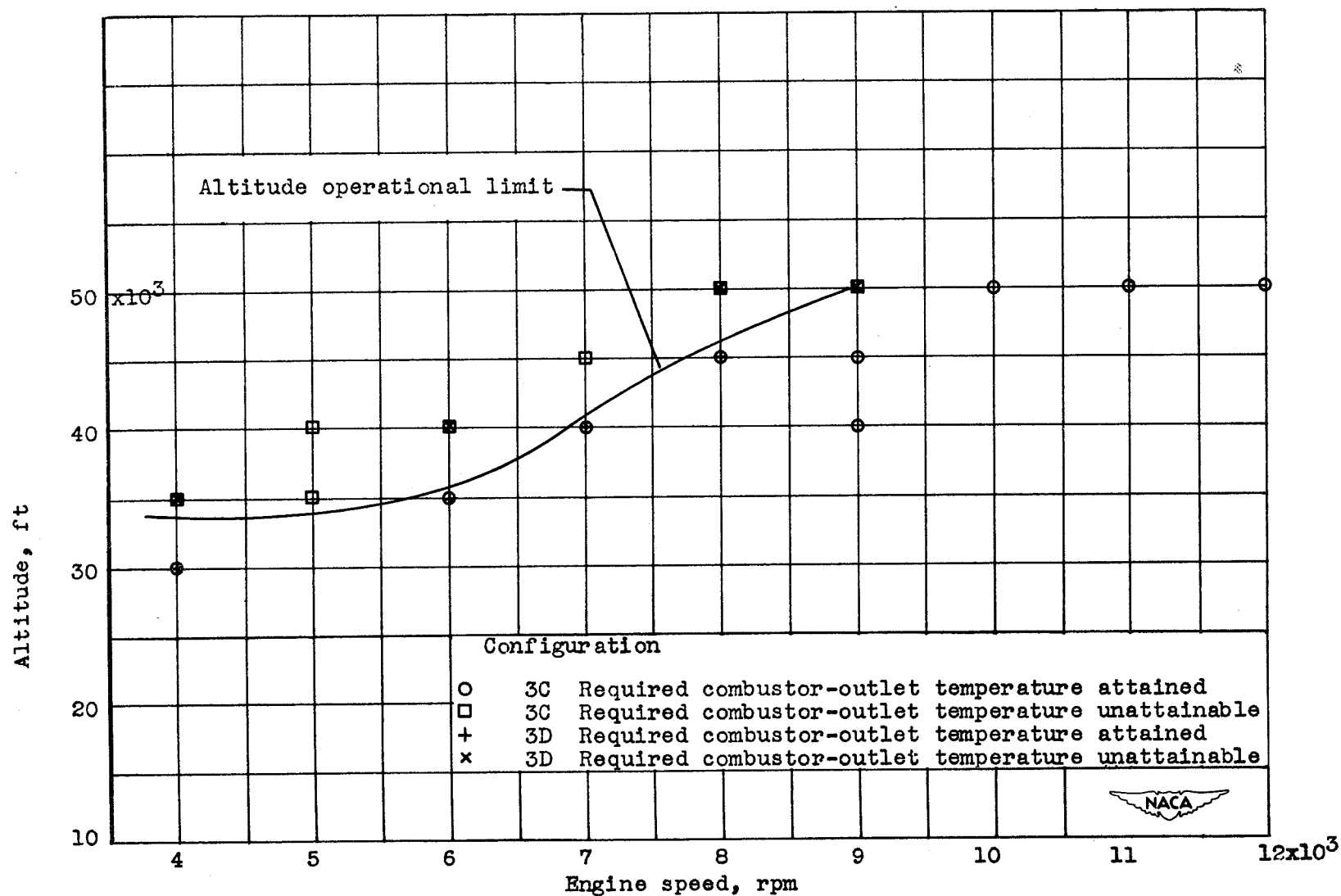
Figure 8. - Continued. Altitude operational limits of 24C jet engine for zero ram as determined with 24C-4 combustor.



(e) Configuration 3A, ram-pressure air holes blocked, and configuration 3B, ram-pressure air holes blocked plus streamlined approach.

Figure 8. - Continued. Altitude operational limits of 24C jet engine for zero ram as determined with 24C-4 combustor.

CONFIDENTIAL



(f) Configuration 3C, ram-pressure air holes and rows of holes on basket blocked, and configuration 3D, streamlined approach plus configuration 3C.

Figure 8. - Concluded. Altitude operational limits of 24C jet engine for zero ram as determined with 24C-4 combustor.

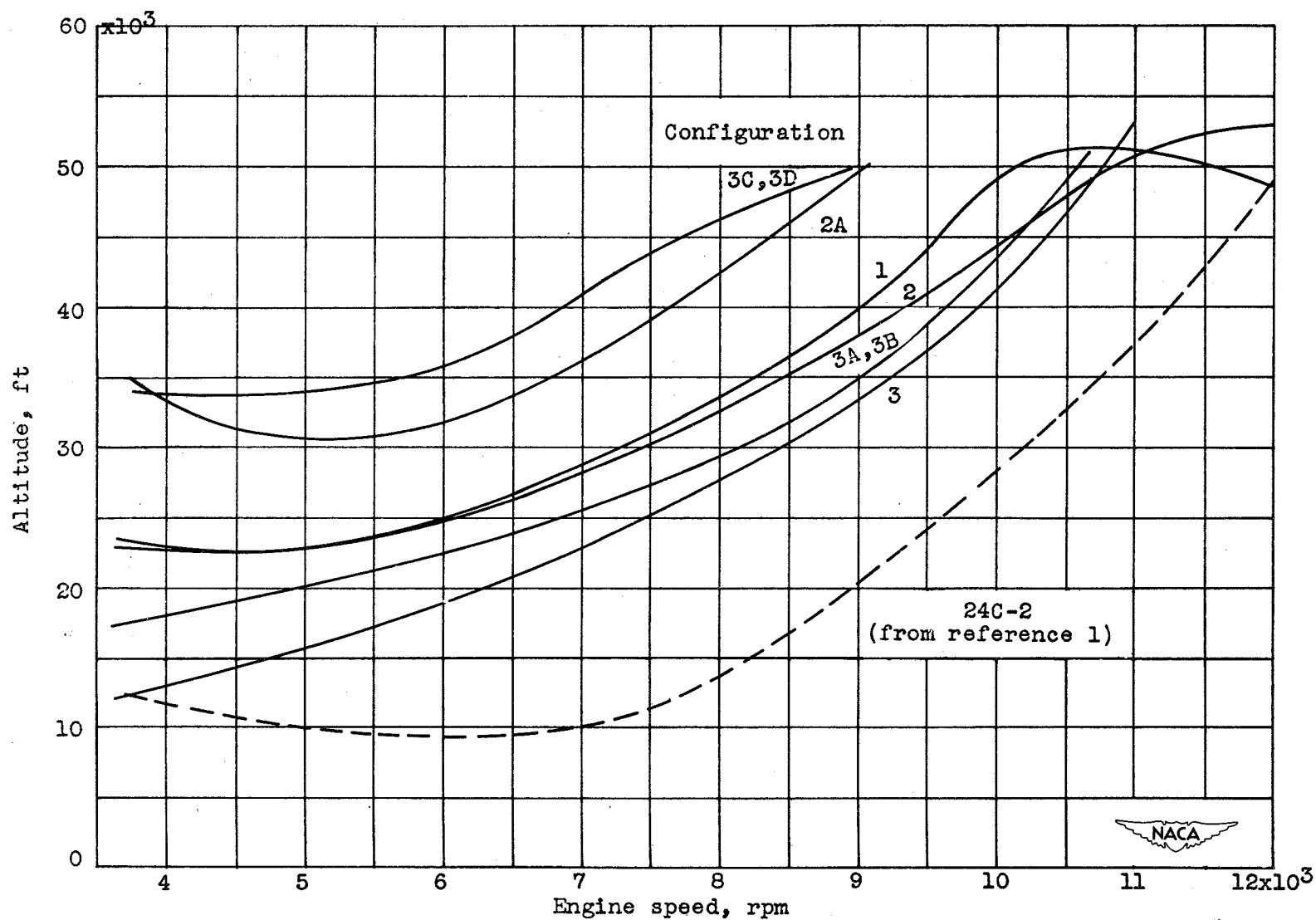


Figure 9. - Comparison of altitude operational limits of 24C jet engine as obtained with 24C-4 combustor using various basket configurations and with 24C-2 combustor.

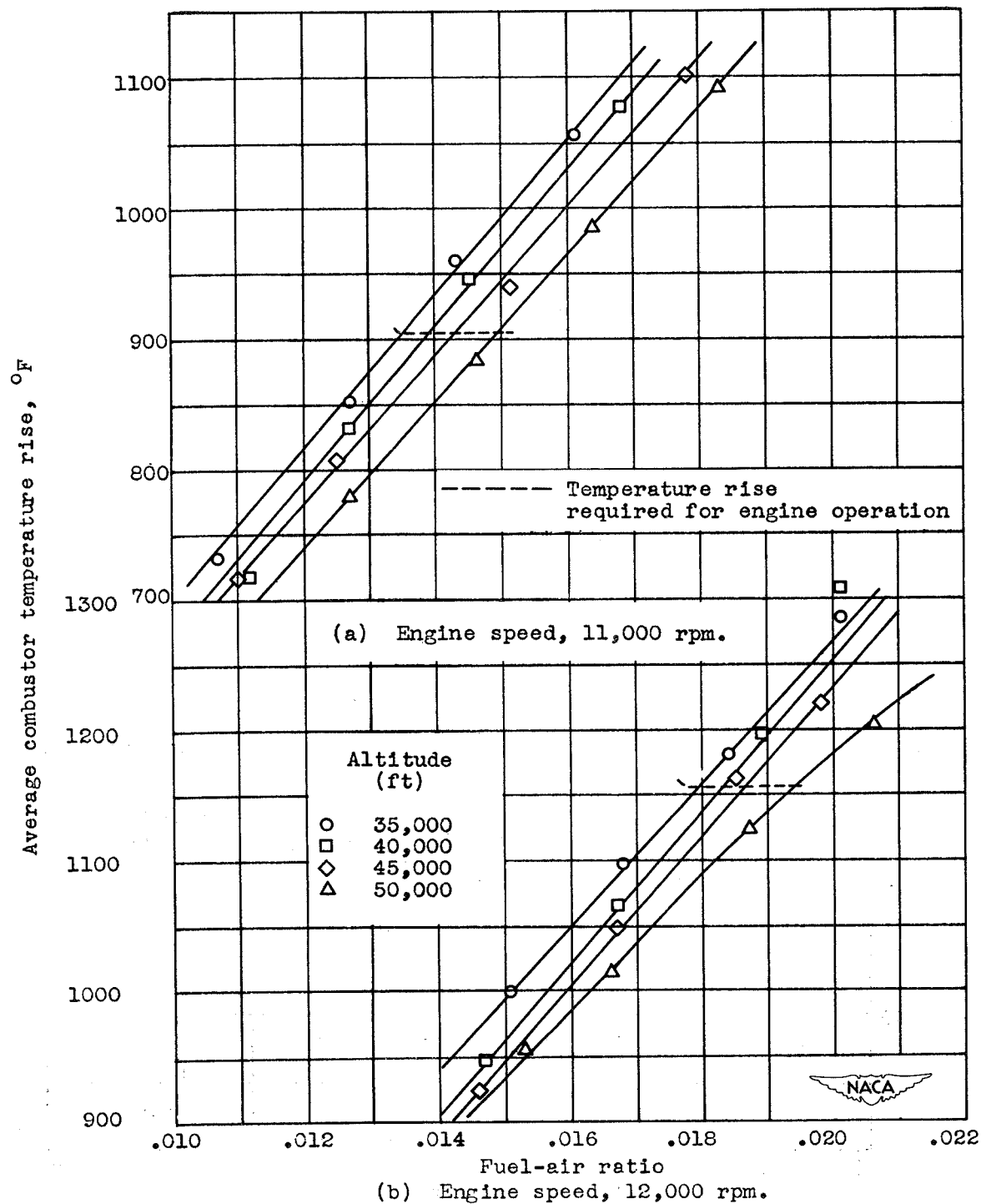
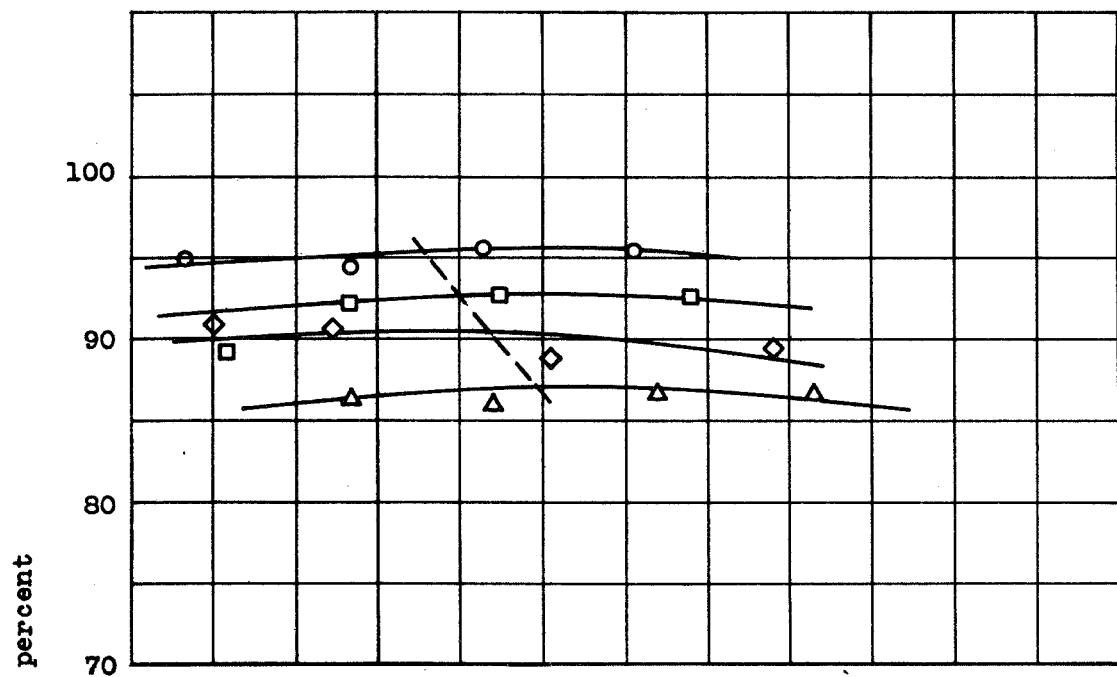
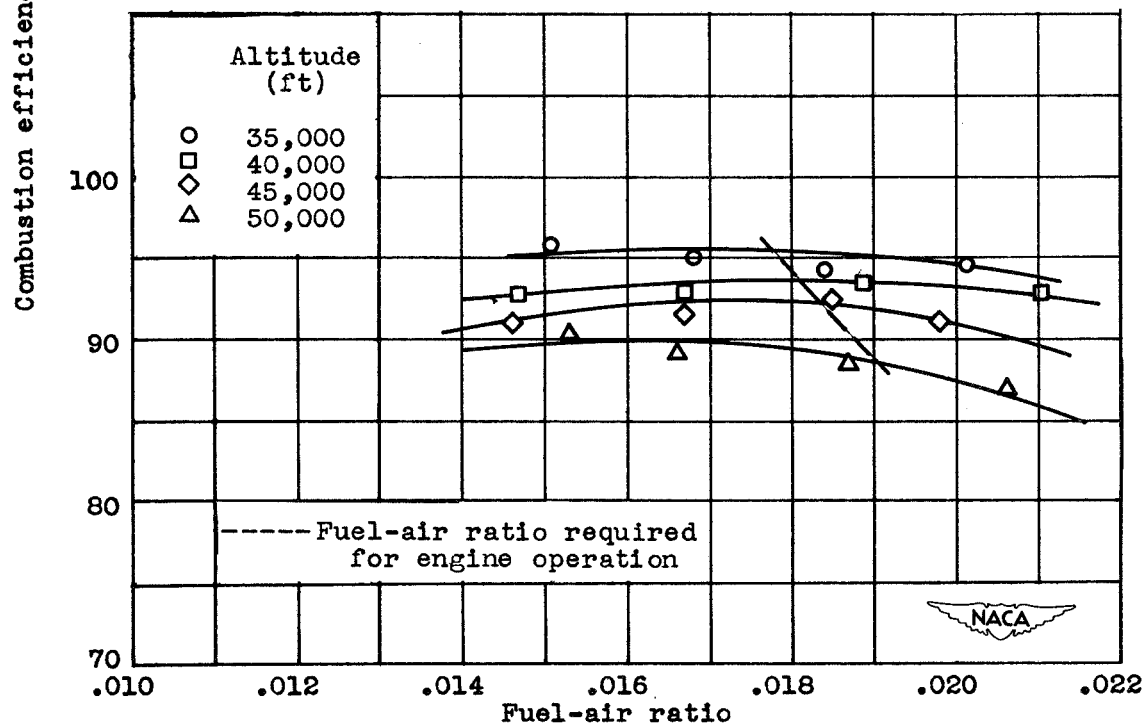


Figure 10. - Variation of average combustor temperature rise with fuel-air ratio for 24C-4 combustor, configuration 3C.

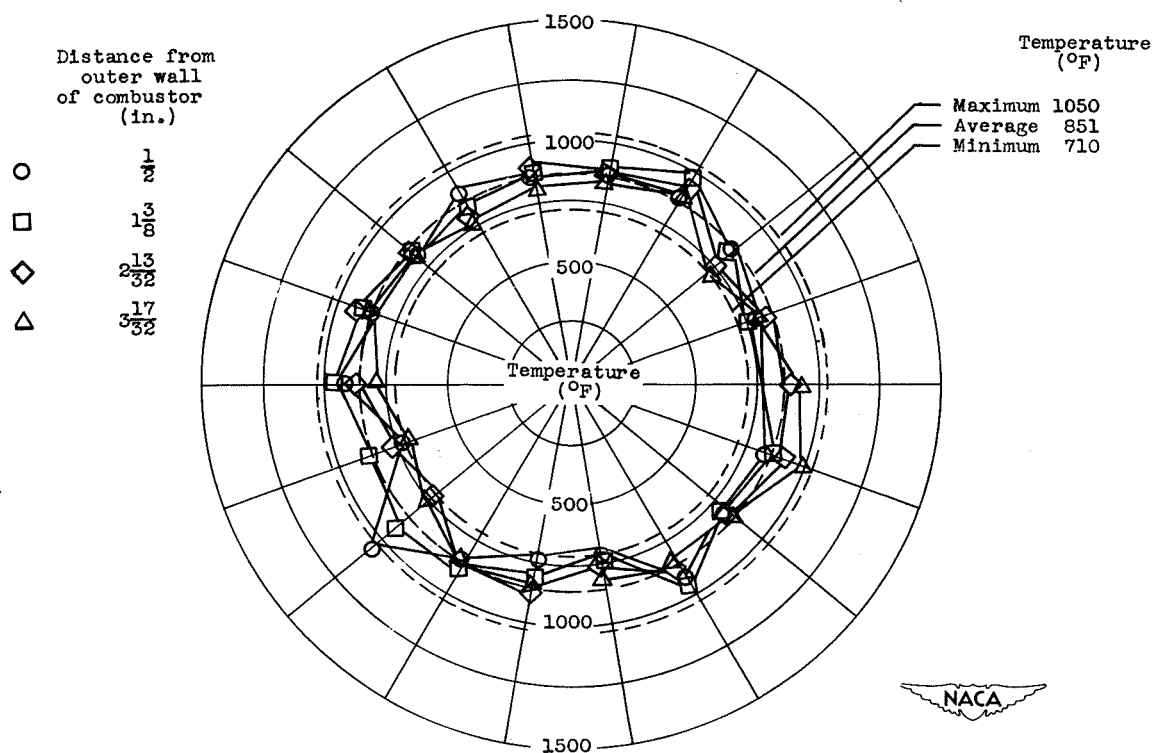


(a) Engine speed, 11,000 rpm.

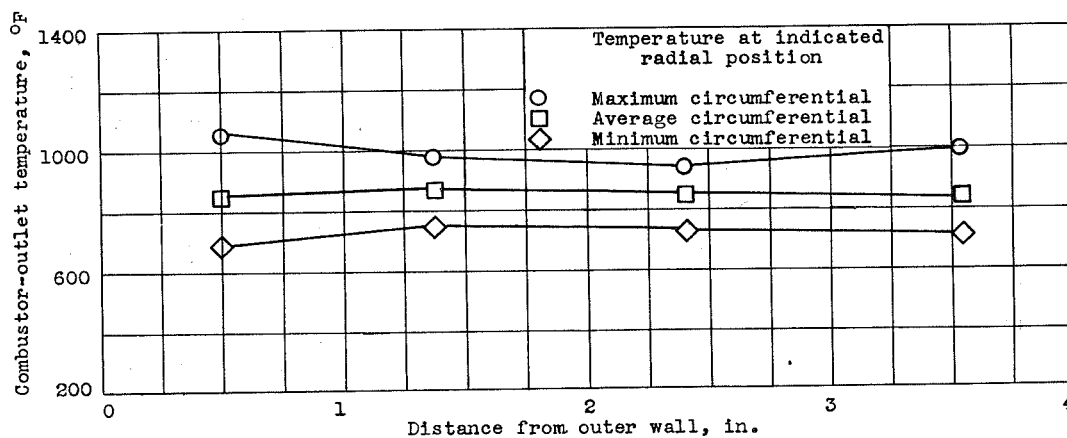


(b) Engine speed, 12,000 rpm.

Figure 11. - Variation of combustion efficiency with fuel-air ratio for 24C-4 combustor, configuration 3C.

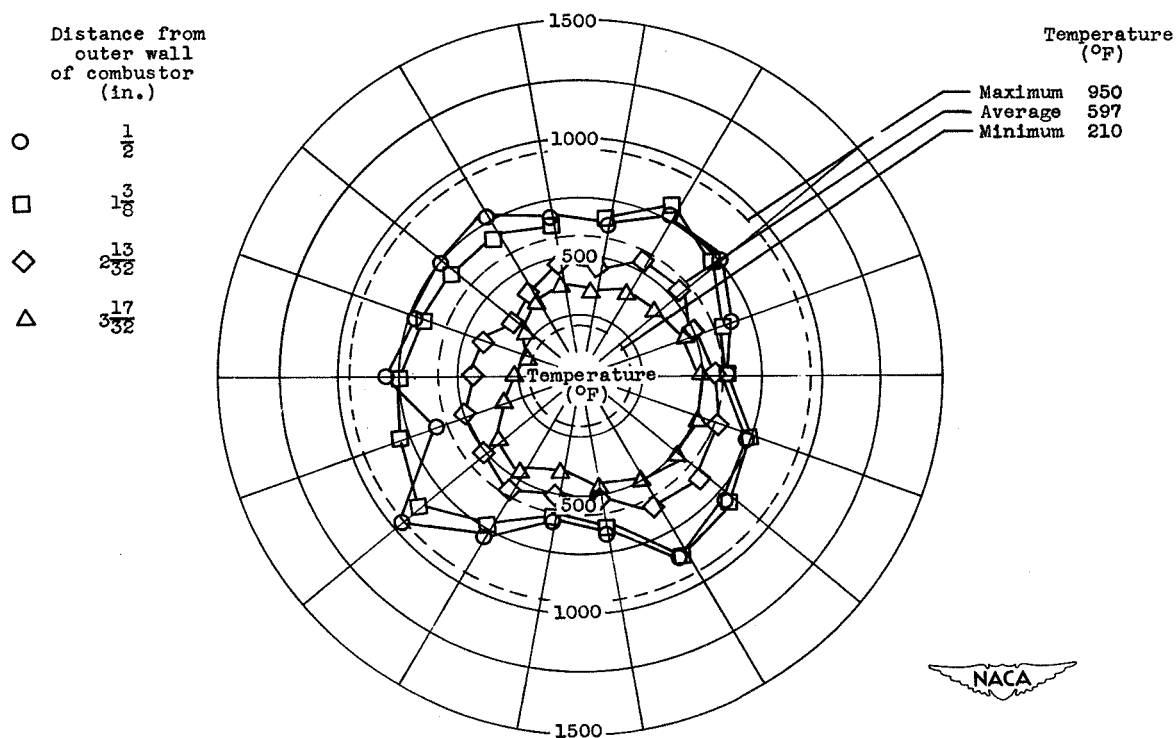


(a) Radial and circumferential temperature distribution during steady combustion; altitude, 22,500 feet.

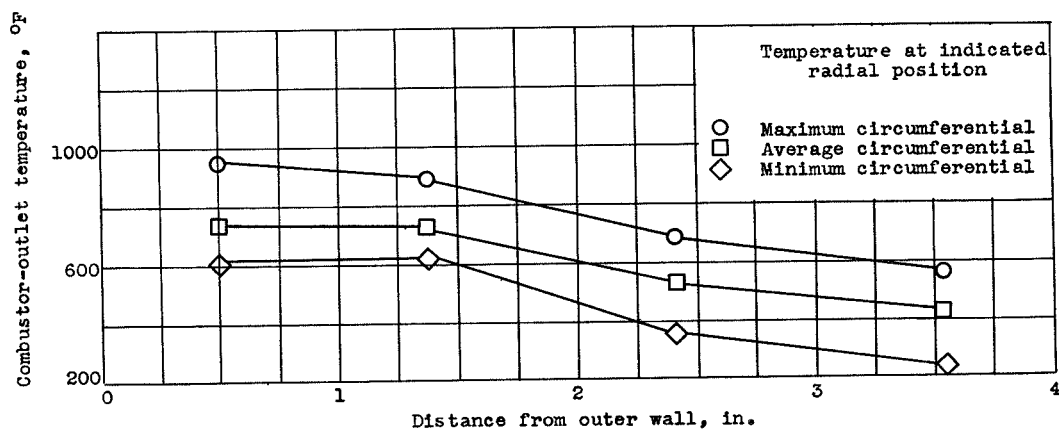


(b) Radial temperature distribution during steady combustion; altitude, 22,500 feet.

Figure 12. - Temperature distribution at combustor outlet (section C-C, looking upstream) during steady and cycling combustion for engine speed of 6000 rpm. 24C-4 combustor, configuration 1.

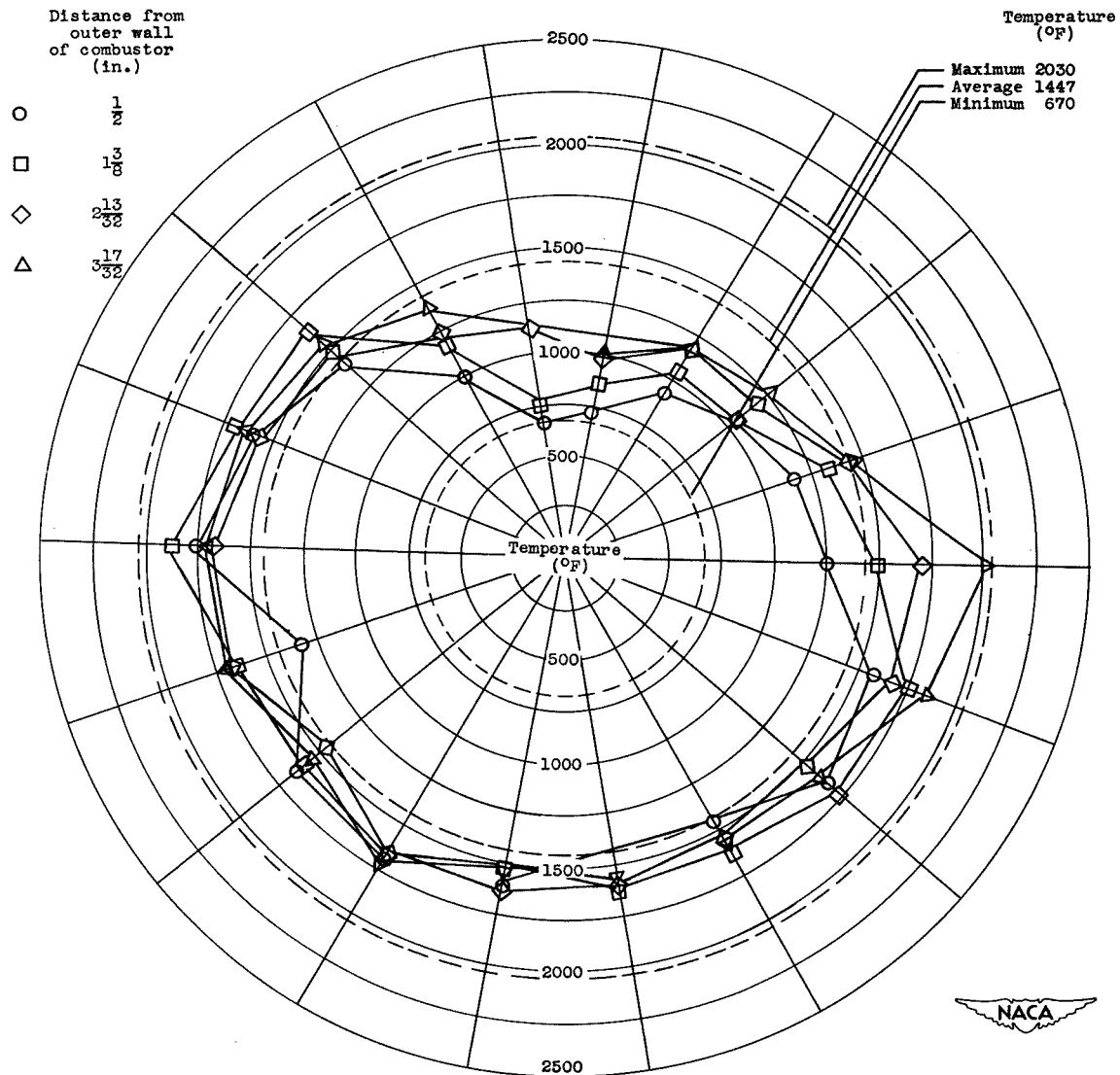


(c) Radial and circumferential temperature distribution during cycling combustion; altitude, 25,000 feet.



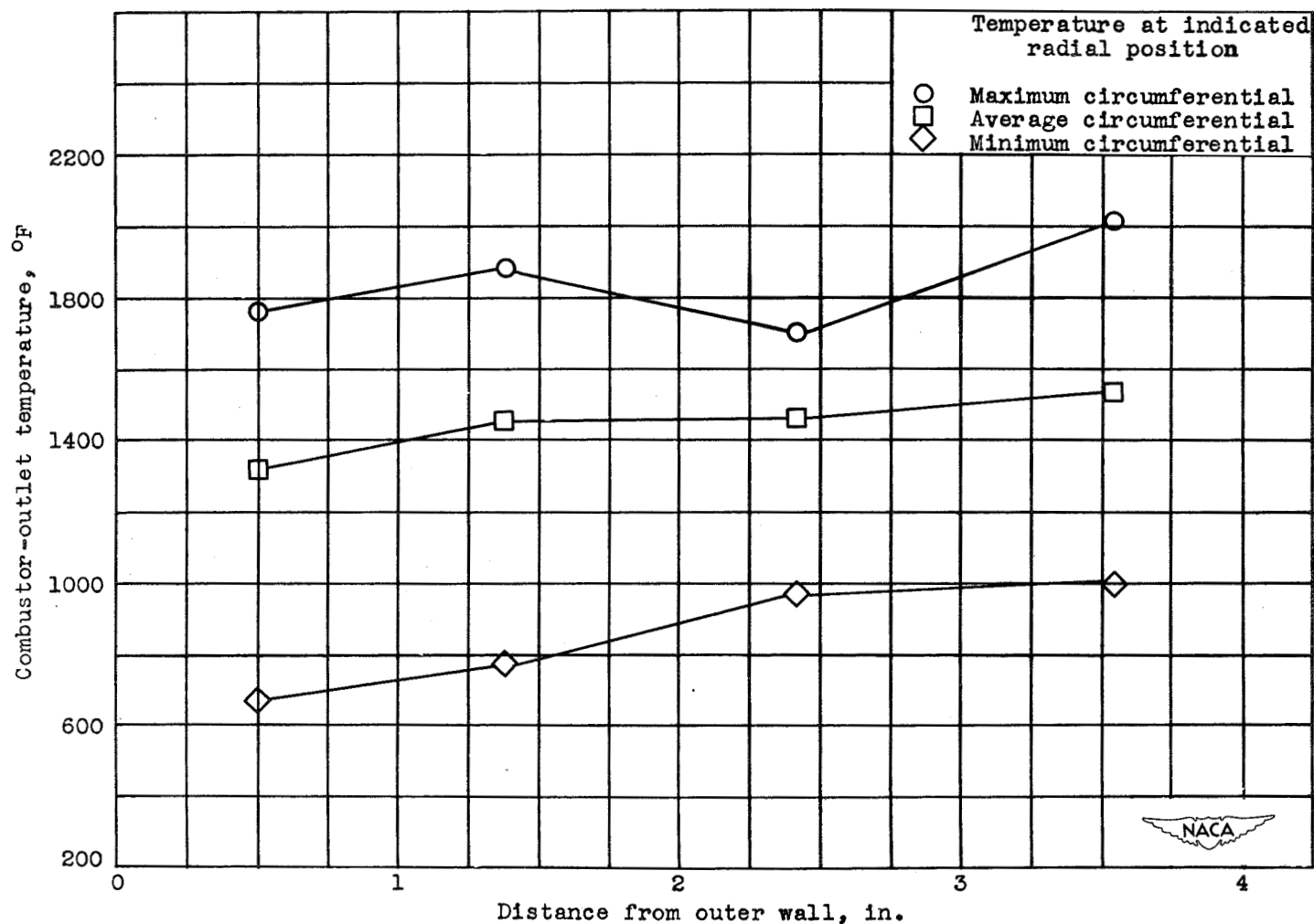
(d) Radial temperature distribution during cycling combustion; altitude, 25,000 feet.

Figure 12. - Concluded. Temperature distribution at combustor outlet (section C-C, looking upstream) during steady and cycling combustion for engine speed of 6000 rpm. 24C-4 combustor, configuration 1.



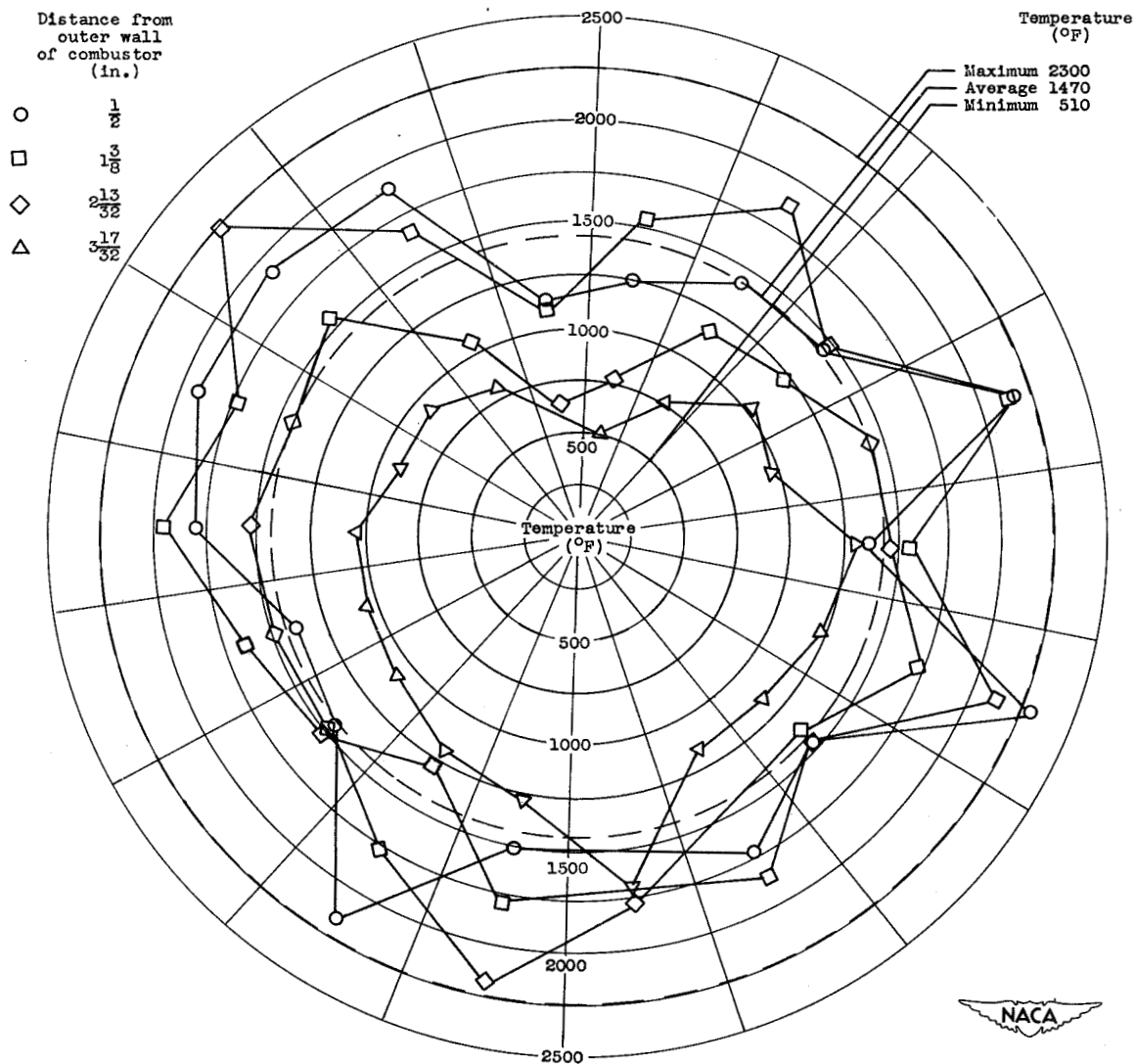
(a) Configuration 2, radial and circumferential temperature distribution.

Figure 13. - Temperature distribution at combustor outlet (section C-C, looking upstream) for high inlet-air temperatures (approximately 280° F) at engine speed of 12,000 rpm and altitude of 50,000 feet. 24C-4 combustor, configurations 2 and 2A.



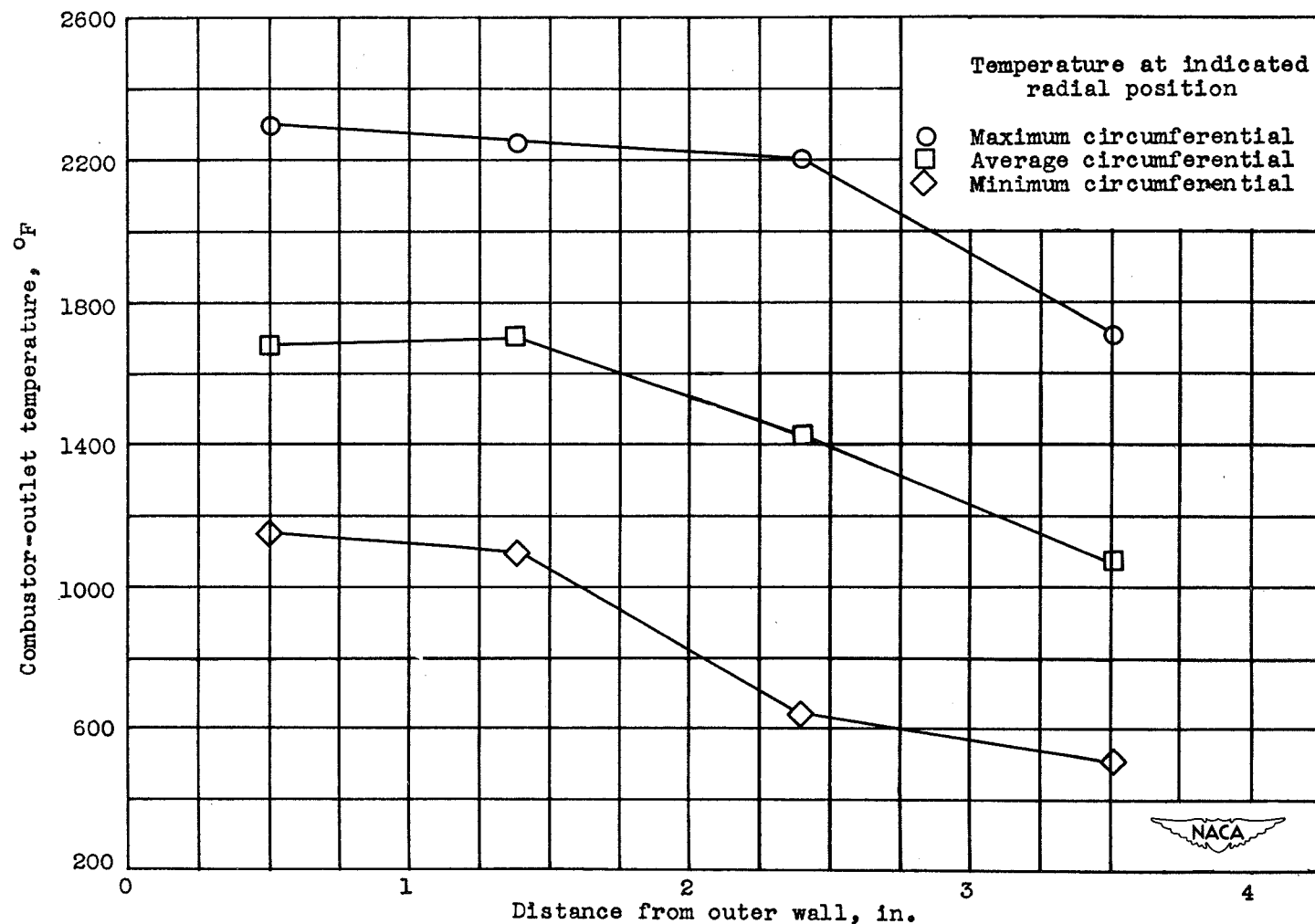
(b) Configuration 2, radial temperature distribution.

Figure 13. - Continued. Temperature distribution at combustor outlet (section C-C, looking upstream) for high inlet-air temperatures (approximately 2800° F) at engine speed of 12,000 rpm and altitude of 50,000 feet. 24C-4 combustor, configuration 2 and 2A.



(c) Configuration 2A, radial and circumferential temperature distribution.

Figure 13. - Continued. Temperature distribution at combustor outlet (section C-C, looking upstream) for high inlet-air temperatures (approximately 280° F) at engine speed of 12,000 rpm and altitude of 50,000 feet. 24C-4 combustor, configurations 2 and 2A.



(d) Configuration 2A, radial temperature distribution.

Figure 13. - Concluded. Temperature distribution at combustor outlet (section C-C, looking upstream) for high inlet-air temperatures (approximately 280° F) at engine speed of 12,000 rpm and altitude of 50,000 feet. 24C-4 combustor, configurations 2 and 2A.

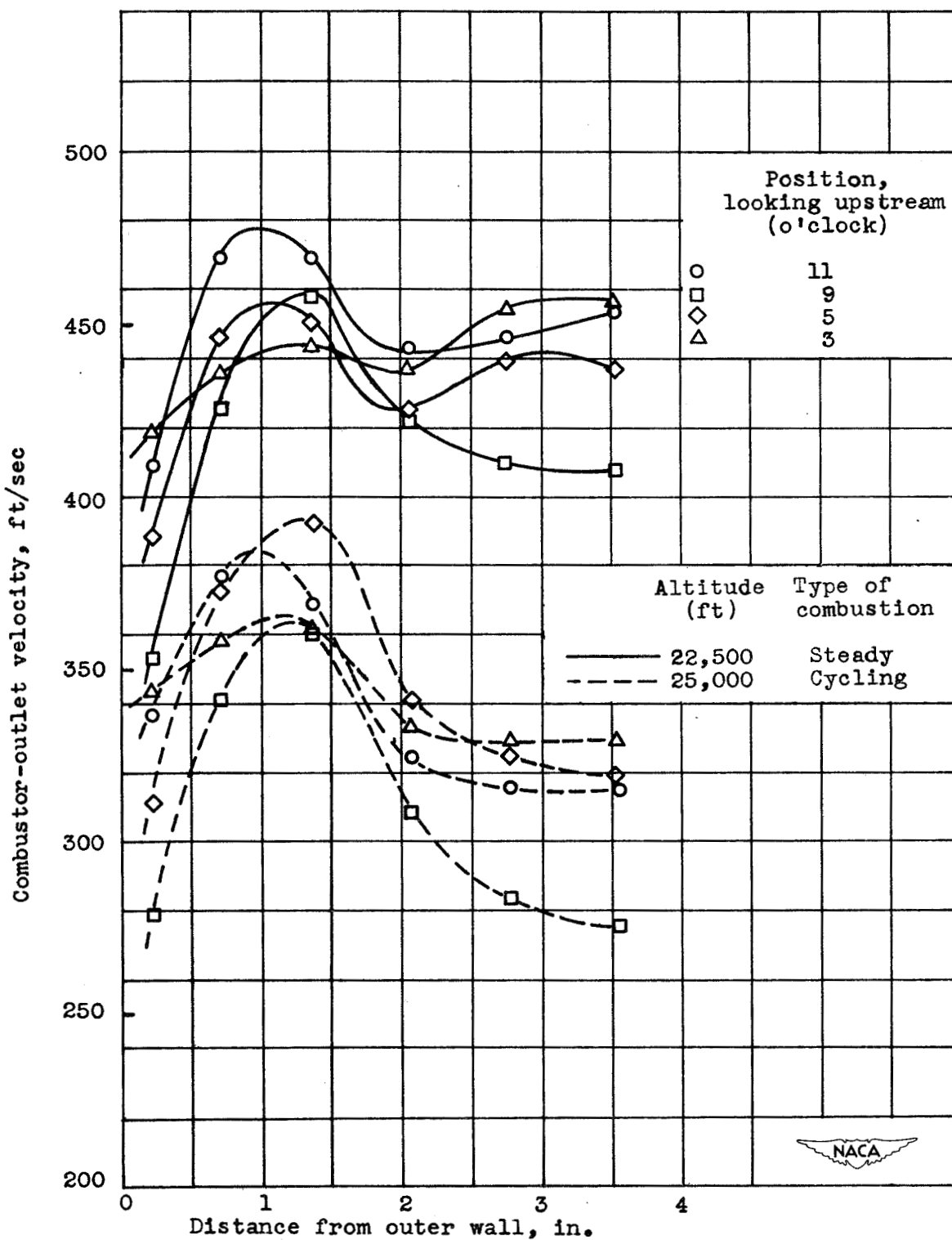
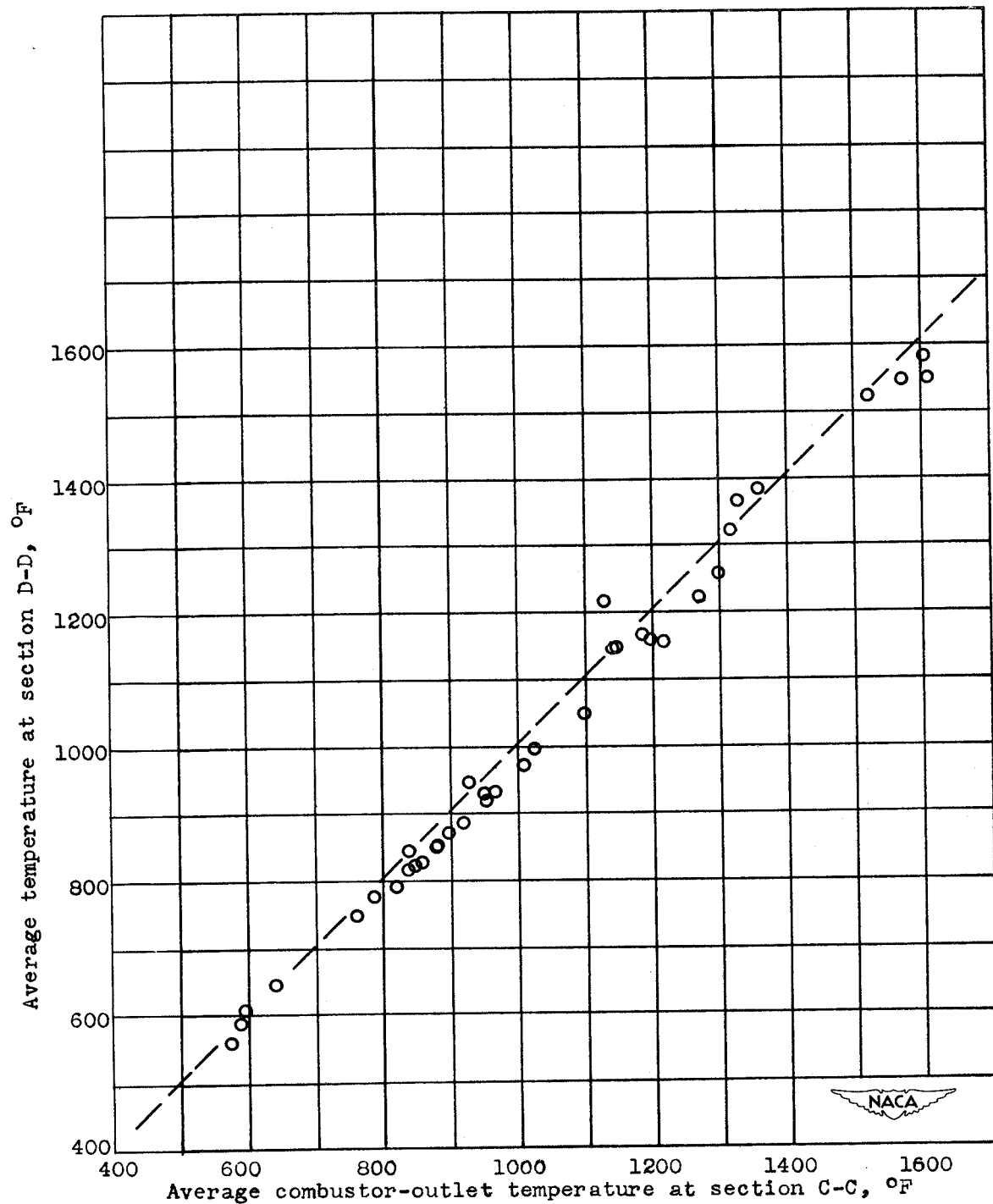


Figure 14. - Velocity distribution at combustor outlet (section C-C).
24C-4 combustor, configuration 1, at an engine speed of 6000 rpm.



(a) Relation of average temperature measured at section D-D to average combustor-outlet temperature.

Figure 15. - Relation of average temperature measured at sections D-D and E-E to average combustor-outlet temperature at section C-C. 24C-4 combustor, configuration 1.

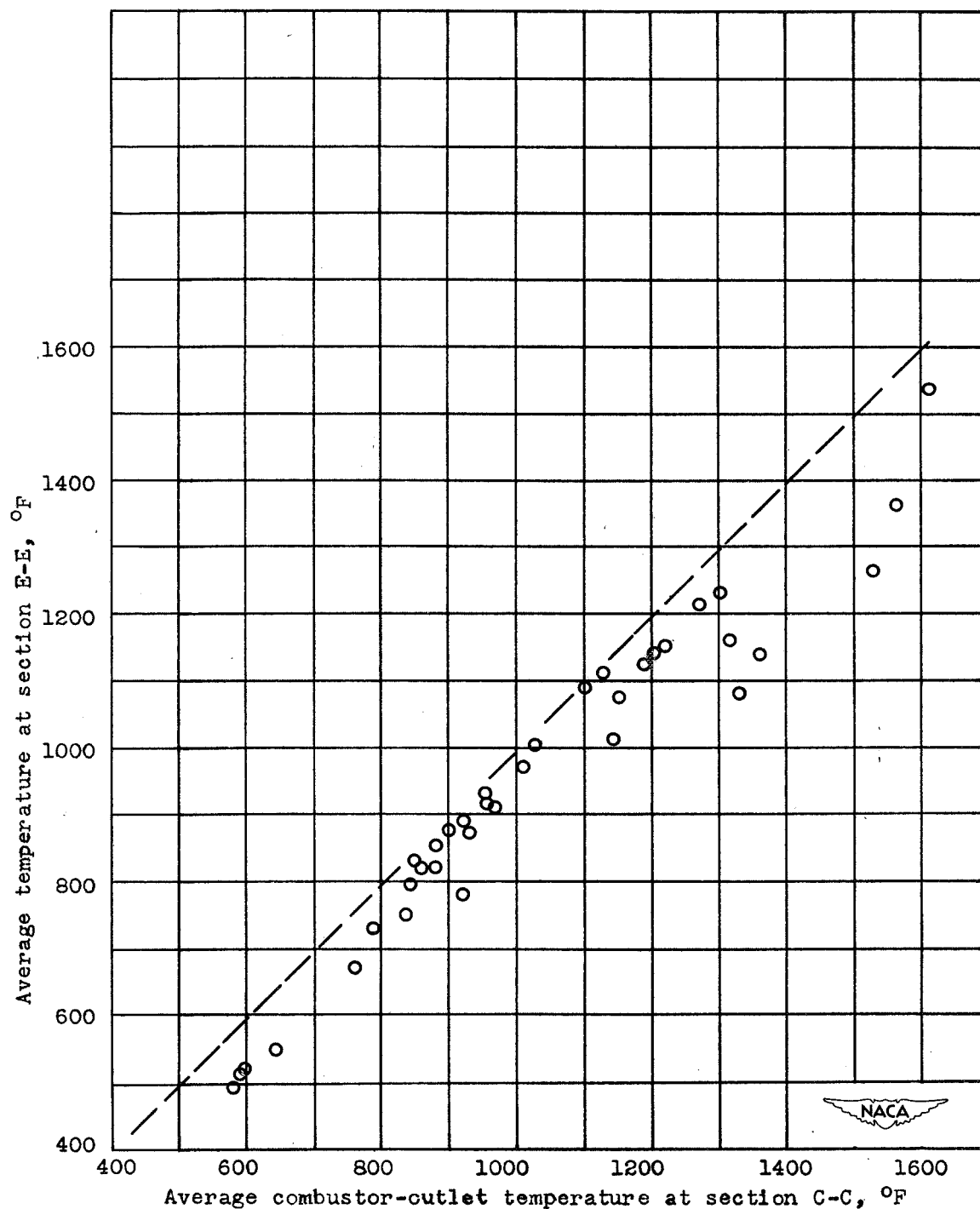


Figure 15. - Concluded. Relation of average temperature measured at sections D-D and E-E to average combustor-outlet temperature at sections C-C. 24C-4 combustor, configuration I.

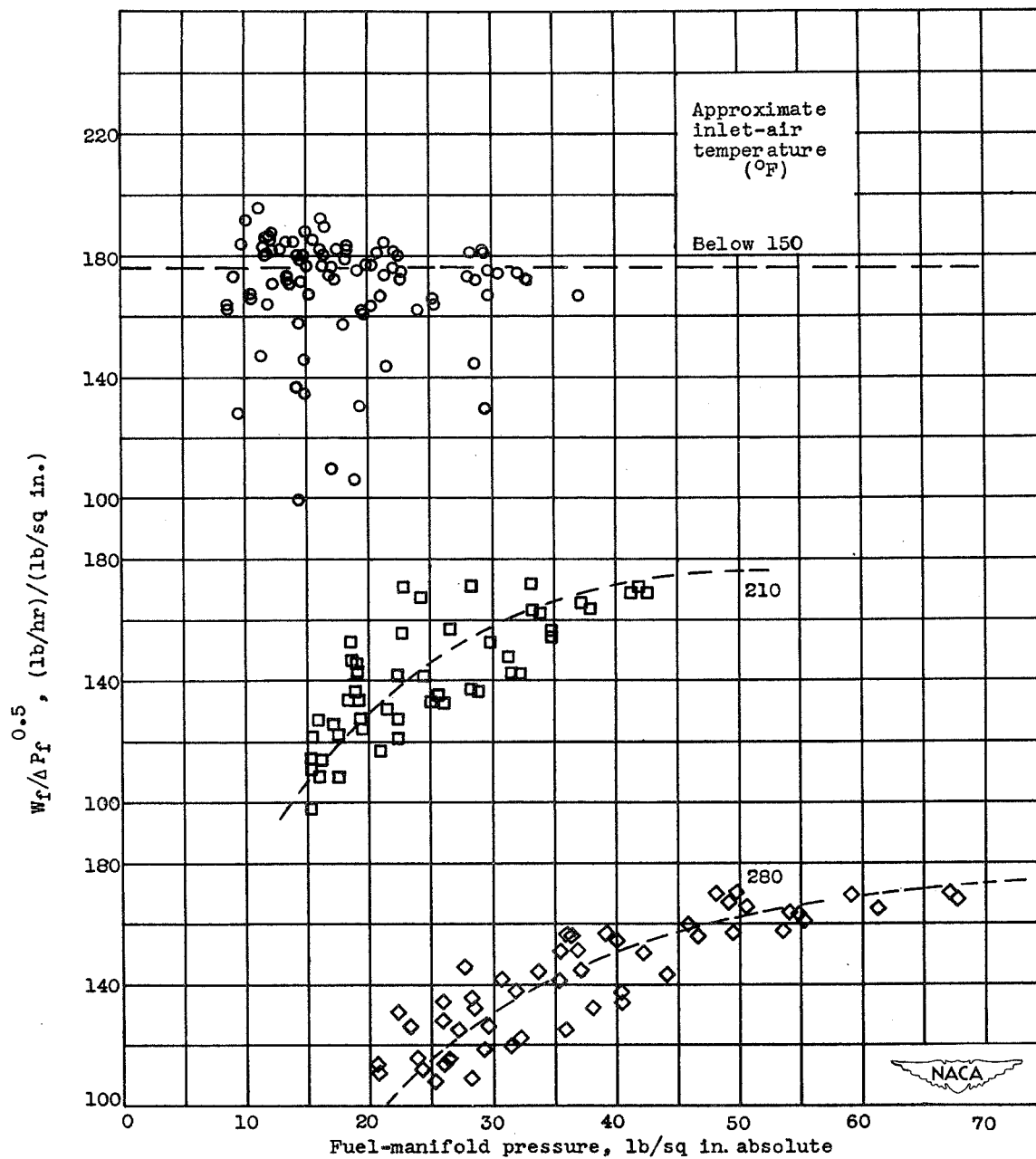
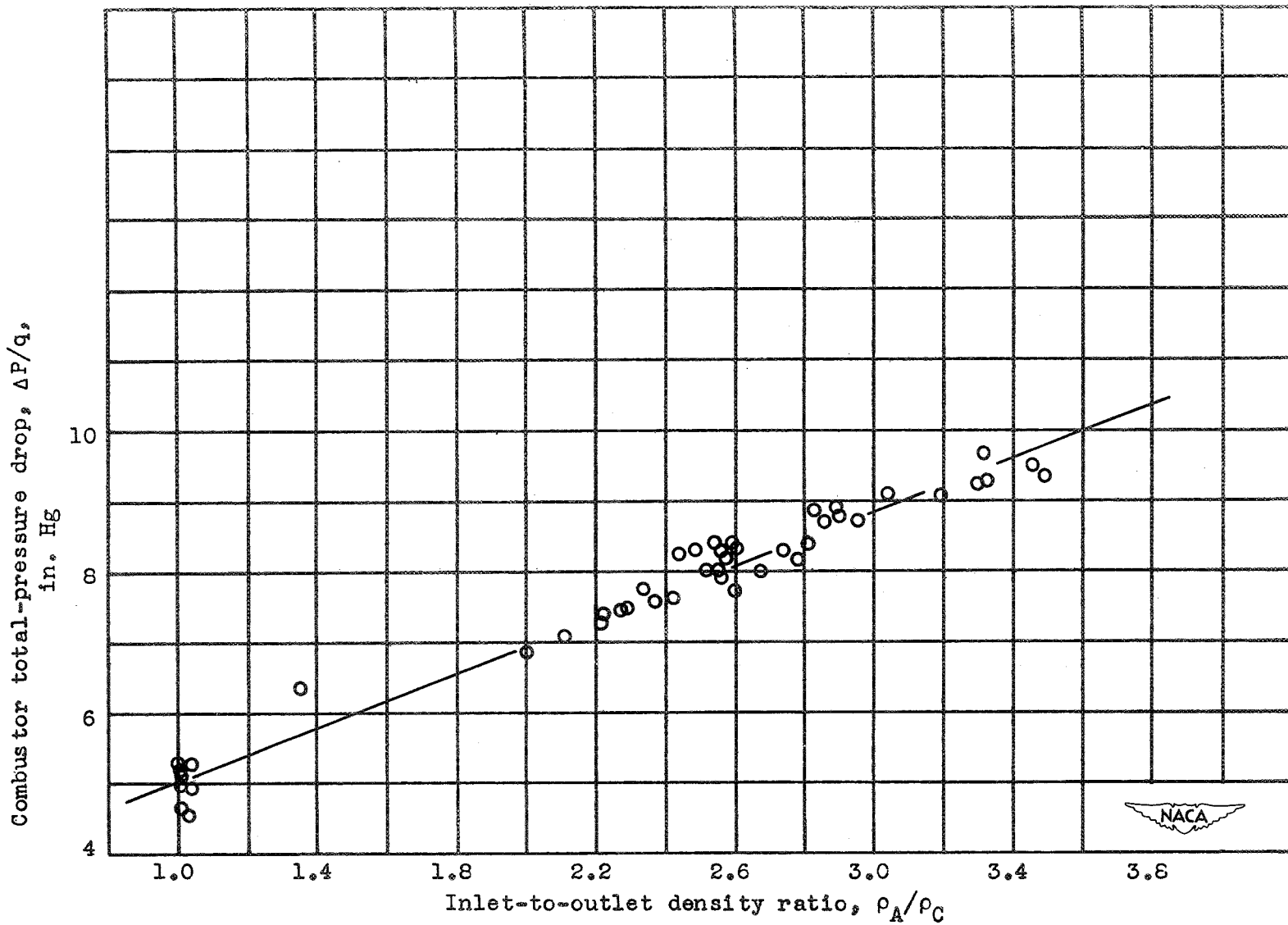


Figure 16. - Fuel-manifold flow characteristics as function of inlet-air temperature. 24C-4 combustor.



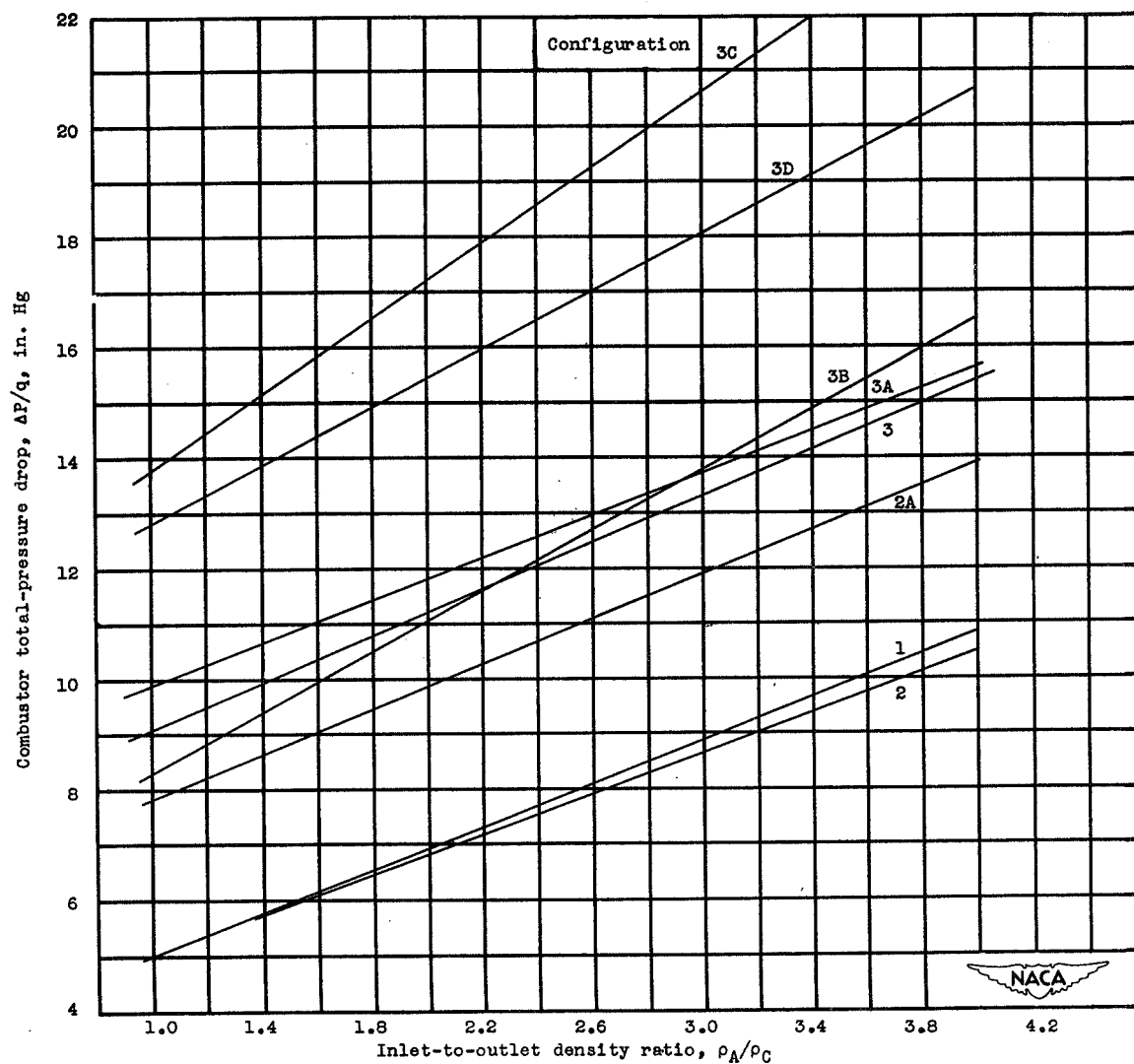


Figure 18. - Comparison of combustor total-pressure drop for 24C-4 combustor baskets and modifications.